NASA CONTRACTOR REPORT

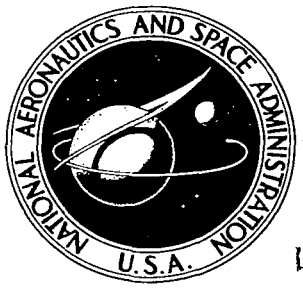

NASA CR-525

CONCEPTUAL DESIGN STUDY FOR A MARS ENTRY VEHICLE DAMPER

by R. A. Winje

Prepared by
TRW SYSTEMS
Redondo Beach, Calif.
for Goddard Space Flight Center

NATIONAL AERONAUTICS AND SPACE ADMINISTRATION • WASHINGTON, D. C. • JULY 1966

NASA CR-525

CONCEPTUAL DESIGN STUDY FOR A MARS ENTRY VEHICLE DAMPER

By R. A. Winje

Prepared under Contract No. NAS 5-9198 by
TRW SYSTEMS
Redondo Beach, Calif.

for Goddard Space Flight Center

NATIONAL AERONAUTICS AND SPACE ADMINISTRATION

For sale by the Clearinghouse for Federal Scientific and Technical Information
Springfield, Virginia 22151 – Price $3.00

ABSTRACT

The results of an analytic study to define a passive damping system to reduce angle-of-attack oscillations of a non-spinning needle-nosed probe entering the Martian atmosphere are presented. The design criteria were generated and then a conceptual design for a passive damping system was developed to satisfy those criteria. In concept, the damping system consists of a mass-spring-dashpot configuration which is tuned to the frequency of angle-of-attack oscillation during the early portion of the entry trajectory. Relative motion between the damper mass and the entry vehicle results in energy dissipation through the dashpot mechanism and inelastic impact at the boundaries of the damper mass excursion. The effectiveness of the system is determined by comparing the damped angle-of-attack envelope to the undamped envelope. Reductions in envelope amplitude of an order of magnitude can be realized with the the damper system.

CONTENTS

ILLUSTRATIONS

TABLES

NOMENCLATURE

A	aerodynamic reference area
A_B	area of bellows
A_N	normal acceleration of entry vehicle
C	degrees centigrade, Compute mode of analog computer operation
C_A	aerodynamic axial force coefficient
C_N	aerodynamic normal force coefficient
C_M	aerodynamic moment coefficient
c	damping coefficient
c_c	"critical" damping coefficient
D	coil diameter of extension spring, diameter of damper housing
D_B	bellows diameter
d	wire diameter of springs, disc diameter
E	modulus of elasticity
F_A	aerodynamic axial force
F_N	aerodynamic normal force
F_ℓ	longitudinal reaction between damper mass and entry vehicle
F	normal reaction between damper mass and entry vehicle
f	undamped natural frequency of damper
G	shear modulus of elasticity
g	acceleration due to planet's gravitational attraction
H	angular momentum, Hold mode of analog computer operation
h_i	entry altitude
h_o	initial altitude at start of analog simulation
h	thickness of damper mass, altitude

I	mass moment of inertia defined by equation 37, area moment of inertia of spiral spring wire
I_1	mass moment of inertia of entry vehicle about its cg
IC	Initial Condition mode of analog computer operation
$\bar{I}, \bar{J}, \bar{K}$	inertial unit vectors
$\bar{i}, \bar{j}, \bar{k}$	body fixed unit vectors
K	spring constant of any one spring
K_T	total spring constant for combination of springs
K_{TA}	total spring constant at location A
K_{TB}	total spring constant at location B
k	spring constant used in analog simulation
L	developed length of spiral spring
L_S	stacked length of bellows
L_E	extended length of bellows
ℓ_{ref}	aerodynamic reference area
ℓ_{cp}	center of pressure location on entry vehicle
ℓ_{cg}	cg location on entry vehicle
M	mass ratio defined by equation 12, bending moment in spiral spring
M_A	aerodynamic moment
m_1	mass of entry vehicle
m_2	damper mass
N	number of coils in spring, number of bellows convolutions
P	load needed to deflect spring a distance Δ
p	pressure

q	dynamic pressure
q_o	initial dynamic pressure at start of analog simulation
$\bar{R}_1$	inertial position vector of entry vehicle cg
$\bar{R}_2$	inertial position vector of damper mass cg
$\bar{R}$	relative position vector of damper mass cg wrt entry vehicle cg
r	longitudinal location of damper mass
$\bar{S}$	relative position vector from combined body cg to entry vehicle cg
S	stroke of bellows, stress in spring
ΔT	temperature range
t	time, thickness of damper housing
V	vehicle entry velocity, volume
V_v	vertical component of entry velocity
ΔV	change of volume
W	weight
x, y	inertial position of entry vehicle
α	angle-of-attack, coefficient of thermal expansion
α_i	entry angle-of-attack
$\dot{\alpha}$	rate of change of angle-of-attack
$\dot{\alpha}_o$	rate of change of angle-of-attack at start of analog simulation
$\ddot{\alpha}$	angular acceleration
$1/\beta$	density scale height of atmosphere
γ	weight density
δ	stroke per convolution of bellows
Δ	spring deflection, gap size

ϵ	coefficient of restitution
ζ	fraction of critical damping
η	damper mass relative displacement
η_M	damper mass maximum relative displacement
$\dot{\eta}$	damper mass relative velocity
$\ddot{\eta}$	damper mass relative acceleration
θ	angle between V and local horizontal
λ	coefficient depending on end conditions of curved beam
μ	coefficient of dynamic viscosity, Poisson's ratio
ν	coefficient of kinematic viscosity
ρ	mass density of atmosphere
ρ_i	atmospheric mass density at entry
σ_{max}	bending stress
σ_{ult}	ultimate stress
ω	frequency

1. INTRODUCTION

The need to reduce or eliminate angle-of-attack oscillations of a hypersonic non-spinning entry vehicle has long been recognized. The reduction or elimination of these oscillations by various active attitude control systems has been accomplished whereas purely passive means for so doing are apparently untried. It was the intent of this study to derive the basic design criteria and to develop a conceptual design of a purely passive system to reduce the angle-of-attack oscillations of a needle-nosed probe entering an assumed Martian atmosphere.

To better understand the development of the study a synopsis of the dynamics of atmospheric entry of a non-spinning vehicle is beneficial. Hypersonic entry of an aerodynamically stable vehicle into an exponential atmosphere causes angle-of-attack oscillations which are convergent. That is, the amplitude of oscillation decreases although the rate increases due to the aerodynamic torques. The rate of change of oscillation frequency depends on the rate of change of the dynamic pressure, which, if velocity is nearly constant, changes with atmospheric density. The density change seen by the vehicle is a result of the density scale height of the atmosphere and/or the vertical component of the entry velocity vector. Thus a grazing entry trajectory will produce less change in oscillation frequency per unit of time than the vertical descent of the same entry vehicle.

These short period oscillations do not couple strongly with the long period trajectory dynamics, however, the oscillations can interfere with communications to and from the vehicle by producing a strong plasma sheath around the vehicle. The desire to reduce the angle-of-attack oscillations of an entry vehicle for communications reasons prompted this study. The vehicle is a needle-nosed probe designed by the Goddard Space Flight Center to collect and transmit data on the Martian atmosphere during its entry. A complete description of the probe and its experiments is given in Reference 1.

To attain the study objectives of establishing design criteria and a conceptual design, the technical approach was as follows. With the basic concept of a sprung mass with damping, the equations of motion for the two body entry into the atmosphere were derived, then damper system parameter ranges and entry trajectory conditions were established so that the equations of motion could be properly scaled for analog computation. Once the equations were programmed, many exploratory analog computer runs were made to establish general trends. With this information a precise matrix of damper system parameters was established for the ensuing analog runs for the several entry conditions. Approximately 500 analog computer trajectories were run and analyzed in detail. From this data damper design criteria were established and, considering other design constraints imposed by the mission, the concept was translated into a design.

2. ANALYSIS

2.1 System Description

The system analyzed is shown schematically in Figure 1. The equations of motion are derived for planar motion and thus there are four degrees of freedom -- three for the entry vehicle and one for the damper mass which is constrained to move normal to the vehicle longitudinal axis. An assumption made in the analysis is that the inertial angular acceleration is equal to the angle-of-attack acceleration, $\ddot{\alpha}$. This assumption is valid for trajectories whose velocity vector is nearly constant. Although there are four degrees of freedom, the equations are finally written in terms of the two coordinates of interest, angle of attack, α, and damper mass relative displacement, η. The damper mass, m_2, is assumed to be a point mass in that its moment of inertia about its own cg is negligible. The term F_η is the force between the vehicle and the damper mass. This force will, in general, be a function of both relative position, η, and relative velocity, $\dot{\eta}$. Now since the damper is constrained to remain interior to the vehicle, there are certain boundary conditions imposed on the damper mass motion. These in turn effect the motion of the entry vehicle. Thus when the damper mass is against the boundary there is no relative motion ($\dot{\eta} = 0$) and η is fixed at $\pm \eta_M$. Let the reaction under these conditions be denoted by F^*_η. The magnitude of the reaction force between the damper mass is then F_η or F^*_η, but not both. For the following derivation, call this reaction F, meaning F_η when mass 2 is not at the boundary and F^*_η when it is on the boundary.

Consider the diagram of Figure 1. Let $\bar{R}_1$ and $\bar{R}_2$ be the inertial positions of mass 1 and mass 2.

Then

$$m_1 \frac{d^2\bar{R}_1}{dt^2} = F_N\bar{j} - F_A\bar{i} + F\bar{j} + F_\ell\bar{i} + m_1 g\bar{I} \qquad (1)$$

$$m_2 \frac{d\bar{R}_2}{dt^2} = - F\bar{j} - F_\ell\bar{i} + m_2 g\bar{I} \qquad (2)$$

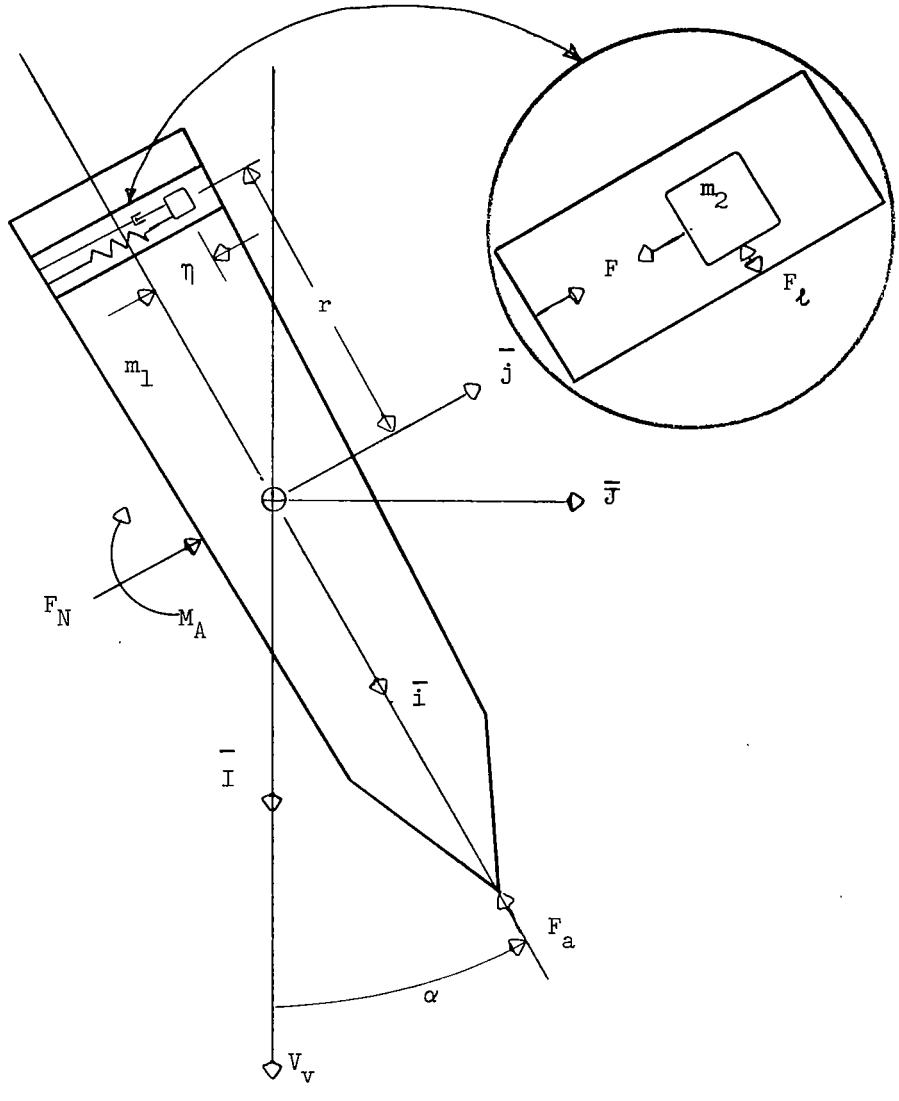

$$\bar{I} = \cos\alpha\ \bar{i} - \sin\alpha\ \bar{j}$$
$$\bar{J} = \cos\alpha\ \bar{j} + \sin\alpha\ \bar{i}$$
$$\bar{i} = \cos\alpha\ \bar{I} + \sin\alpha\ \bar{J}$$
$$\bar{j} = \cos\alpha\ \bar{J} - \sin\alpha\ \bar{I}$$

FIGURE 1 Probe Geometry & Coordinate System

$$I_1\ddot{\alpha} = -M_A - \eta F_\ell - rF \tag{3}$$

performing the indicated differentiations on Equations (1) and (2) and writing in component form gives

for body 2

$$m_2 (\ddot{x} \cos \alpha + \ddot{y} \sin \alpha + r\dot{\alpha}^2 - 2\dot{\alpha}\dot{\eta} - \eta\ddot{\alpha}) =$$

$$-F_\ell + m_2 g \cos \alpha \tag{4}$$

$$m_2 (-\ddot{x} \sin \alpha + \ddot{y} \cos \alpha + \ddot{\eta} - r\ddot{\alpha} - \eta\dot{\alpha}^2) =$$

$$-F - m_2 g \sin \alpha \tag{5}$$

and for body 1

$$m_1\ddot{x} = -(F_N + F) \sin \alpha - (F_A - F_\ell) \cos \alpha + m_1 g \tag{6}$$

$$m_2\ddot{y} = (F_N + F) \cos \alpha - (F_A - F_\ell) \sin \alpha \tag{7}$$

eliminate $\ddot{x}$ and $\ddot{y}$ by substituting from (6) and (7) into (4) and (5) to give

$$m_2 \left[+r\dot{\alpha}^2 - 2\dot{\alpha}\dot{\eta} - \eta\ddot{\alpha} - \left(\frac{F_A - F_\ell}{m_1} \right) \right] = - F_\ell \tag{8}$$

$$m_2 \left[\ddot{\eta} - r\ddot{\alpha} - \eta\dot{\alpha}^2 + \left(\frac{F_N + F}{m_1} \right) \right] = - F \tag{9}$$

Now eliminate F_ℓ between (3), (8), and (9) to give the governing differential equations in the coordinates of interest α, η.

$$\ddot{\eta} - r\ddot{\alpha} - \dot{\alpha}^2\eta = -\frac{F_N}{m_1} - \frac{F}{M} \tag{10}$$

$$I_1 + M (\eta^2 + r^2) \ddot{\alpha} = - M_A - \frac{M}{m_1} (\eta F_A - rF_N) + rM\ddot{\eta} - 2\eta\dot{\eta}\dot{\alpha}M \tag{11}$$

where

$$M = \frac{m_1 m_2}{m_1 + m_2} \tag{12}$$

It now must be remembered that F is either F_η of F_η^* depending on whether or not the damper mass has reached a boundary. If the mass is at boundary then $\dot{\eta}$ and $\ddot{\eta}$ are zero and the last two terms on the right hand side of Equation (11) are zero. In this study the force F results from the action of a spring and/or dashpot so that

$$F_\eta = + c\dot{\eta} + k\eta$$

where c is a damping coefficient and

k is a spring rate

Equations (10) and (11) describe the motion when the damper mass is on or off the boundary. The impact of the damper mass on the boundary wall requires another set of equations. Since the impact is internal to the two-body system angular momentum is conserved and the necessary expressions are derived from this principle. Remembering that only planar motion is considered there is but one component of angular momentum - that normal to the plane of motion.

The angular momentum, H, about the combined cg is

$$H = I_1\dot{\alpha} + \bar{S}xm_1\left(\bar{V}_{cg} + \frac{d}{dt}\bar{S}\right) + (\bar{R} + \bar{S}) \times m_2\left\{\bar{V}_{cg} + \frac{d}{dt}(\bar{R} + \bar{S})\right\} \tag{13}$$

where

$\bar{S}$ = distance from combined cg to body 1 cg

$\bar{R} + \bar{S}$ = distance from combined cg to body 2 cg

$\bar{V}_{cg}$ = inertial velocity of combined cg

x = the vector cross product operator and the resultants of the operations in Equation (13) are normal to the plane of motion.

However from the definition of combined cg

$$\bar{S}m_1 + (\bar{S} + \bar{R})\, m_2 = 0 \tag{14}$$

Therefore upon substituting (12) and (14) into (13)

$$H = I_1\dot{\alpha} + M\,(\bar{R} \times \frac{d}{dt}\bar{R}) \tag{15}$$

from Figure 1,

$$\bar{R} = -r\bar{i} + \eta\bar{j} \tag{16}$$

$$\frac{d}{dt}\bar{R} = -\dot{\alpha}\eta\bar{i} + (\dot{\eta} - r\dot{\alpha})\,\bar{j} \tag{17}$$

$$\bar{R} \times \frac{d}{dt}\bar{R} = (-r\dot{\eta} + r^2\dot{\alpha} + \dot{\alpha}\eta^2)\,\bar{k} \tag{18}$$

Substituting (18) into (15) gives

$$H = \{I_1 + M\,(r^2 + \eta^2)\}\,\dot{\alpha} - rM\dot{\eta} \tag{19}$$

Conservation of angular momentum before and after impact at $\eta = \pm\,\eta_M$ then gives

$$\{I_1 + M\,(r^2 + \eta_M^2)\}\,\dot{\alpha}_a - rM\dot{\eta}_a = \{I_1 + M\,(r^2 + \eta_M^2)\}\,\dot{\alpha}_b - rM\dot{\eta}_b \tag{20}$$

where the a and b subscripts represent after and before impact respectively.

Now at the time of impact there is deformation and restoration of both the damper mass and the boundary. To circumvent the complex mathematics involved in defining this interaction at impact, the coefficient of restitution, ϵ, is introduced. It is defined such that the velocity of separation is some fraction, ϵ, of the velocity of approach. That is

$$V_{\text{separation}} = \epsilon V_{\text{approach}} \tag{21}$$

where

$$0 \le \epsilon \le 1$$

Thus what are really considered are the motions just before and just after the impact phenomenon occurs. This will be valid since the time involved in the impacting is small compared to other pertinent times in the system. If the coefficient of restitution is equal to unity the collision is perfectly elastic and no energy is lost (i.e. a ball dropped from height h would rebound to height h). If on the other hand ϵ is less than one, some energy is transformed to another form and the total system mechanical energy has been reduced.

Since η is a relative coordinate the following holds

$$\dot{\eta}_a = - \epsilon \dot{\eta}_b \tag{22}$$

where again the a and b subscripts represent after and before impact respectively.

Substituting (22) into (20) and rearranging, the expression for $\dot{\alpha}$ after the impact in terms of rates before impact is

$$\dot{\alpha}_a = \dot{\alpha}_b - \frac{rM\ (1 + \epsilon)}{I_1 + M\ (r^2 + \eta_M^2)}\ \dot{\eta}_b \tag{23}$$

Thus Equations (22) and (23) define the step change in coordinate rates at impact. These in conjunction with Equations (10) and (11) describe the system dynamics.

2.2 System Parameters

In preparation of the system equations for the analog computer it is necessary to examine the actual numbers to be used, since in analog work floating point arithmetic is not available. In analog work, problem variables are represented by voltages which usually are limited to $\pm$ 100 volts. The range in simulations then is restricted to about a factor of 200 assuming reliably accurate operation at .5 volts. To discuss the system properties, it is convenient to divide them into three groups; probe properties, trajectory parameters, and damper system properties.

The probe mass and inertia properties are from References 1 and 2 and are listed in Table I.

TABLE I PROBE MASS PROPERTIES

$m_1 = 1.88$ slugs	this includes all but the weight of the damper mass of the damper system
$I_1 = 1.47$ slug-ft^2	this inertia is about the c.g. of body 1 and includes all but the movable mass of the damper system
$r = .917$ ft	this is distance from body 1 c.g. to m_2 along the longitudinal axis
$\eta_M = 1.5$in & 5in	this is $\frac{1}{2}$ the actual free travel motion permitted, two separate free travel lengths were considered.
$A = .567$ ft^2	this is the aerodynamic reference area
$\ell_{ref} = 1$ ft	this is the reference length taken to be 1 ft in the aerodynamic moment coefficient calculation

The aerodynamics of the probe vehicle are given in terms of an axial force coefficient, C_A; a normal force coefficient, C_N; and a center of pressure location measured from the nose, ℓ_{cp}. The center of pressure location was differenced with the cg location of body 1 (assumed constant) and a moment coefficient about the cg generated by the following expression.

$$C_M = C_N \frac{\ell_{cp} - \ell_{cg}}{\ell_{ref}} \tag{24}$$

The aerodynamic axial force, normal force, and moment are then given by

$$F_A = C_A qA \quad = \text{axial force} \tag{25}$$

$$F_N = C_N qA \quad = \text{normal force} \tag{26}$$

$$M_A = C_M q \ell_{ref} A \quad = \text{moment} \tag{27}$$

where q is dynamic pressure.

At hypersonic speeds these coefficients are a function of angle-of-attack only and are given in Figure 2.

The only trajectory parameter of interest is dynamic pressure, q, and its variation. Dynamic pressure q is defined as

$$q = \tfrac{1}{2} \rho V^2 \tag{28}$$

where V = velocity relative to the atmosphere

ρ = mass density of the atmosphere

With the assumption of an exponential atmosphere, mass density is given by

$$\rho = \rho_s e^{-\beta h} \tag{29}$$

where ρ_s = surface density

$1/\beta$ = density scale height

h = altitude

With the assumption of constant velocity, h can be written as

$$h = h_i - V_v t \tag{30}$$

where h_i is the initial altitude and V_v is the vertical component of velocity. Thus ρ can be written as

$$\rho = \rho_s e^{-\beta (h_i - V_v t)} \tag{31}$$

$$\rho = \rho_s e^{-\beta h_i} e^{\beta V_v t} \tag{32}$$

$$\rho = \rho_i e^{\beta V_v t} \tag{33}$$

where

$$\rho_i = \rho_s e^{-\beta h_i}$$

is the value of density at the initial altitude.

Therefore q can be written as

$$q = \tfrac{1}{2} \rho_i V^2 e^{\beta V_v t} = q_i e^{\beta V_v t} \tag{34}$$

For this study the engineering model atmosphere #3 was used (Reference 3). For this atmosphere and altitudes above 75,000 feet the density scale height is 21,000 ft. Three entry velocities were considered during the study. They were 21,800 ft/sec, 19,200 ft/sec and 15,000 ft/sec. The first two of these entries were vertical, $\theta = 90°$, while the latter was a grazing entry, $\theta = 16°$.

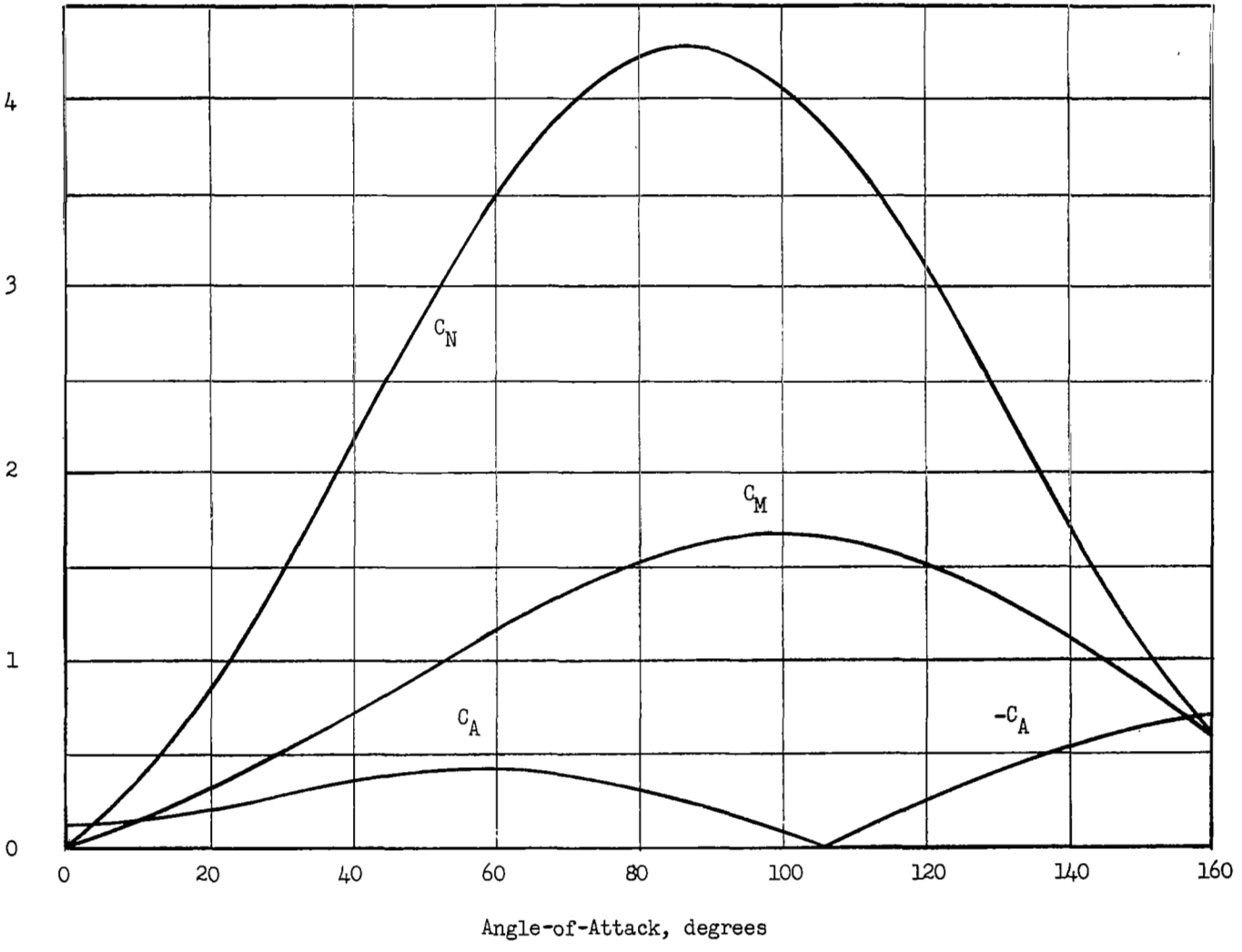

FIGURE 2 Probe Aerodynamic Coefficients

The outer extremities of the assumed Martian atmosphere were approximately 543,000 feet. For a given trajectory (i.e. entry angle, velocity, etc.) the angle-of-attack envelope is determined by the initial angle-of-attack at entry (180°-backwards, 90°-broadside, etc). Also, other studies have shown that small initial angular rates do not significantly affect this envelope. As a baseline, trajectories with no damper and initial angles-of-attack of 155° were run and the first zero crossing of α noted. This data was provided by NASA/Goddard Space Flight Center as Reference 2.

The simulations in the study began at the first zero crossing from these trajectories. From these three trajectories (15,000 ft/sec, 19,200 ft/sec and 21,800 ft/sec), at 155° entry angle-of-attack at 543,000 ft, the angular rates at the first zero crossing were extracted and the analog studies initiated. In addition to these three basic runs, the angular rates were reduced by several factors and more trajectories simulated. These reduced angular rate cases would then correspond to lower (than 155°) entry angles-of-attack at 543,000 feet. Table II gives the trajectories that were considered. The subscript "i" refers to the entry condition at 543,000 feet. The subscript "o" refers to the condition of the first α zero crossing and thus the initiation of the analog study.

The damper system parameters are mass, damping, frequency, coefficient of restitution and free travel length. From the exploratory studies the heavier damper mass gave better angle-of-attack reduction. Since the total damper system was to weigh approximately six pounds, a four pound damper mass was assumed. All results presented herein are with a damper mass of four pounds. Since the frequency of oscillation increases with entry into the atmosphere several values of undamped natural frequency of the damper were studied. With a mass and an undamped natural frequency, several values of a viscous damping coefficient were used. Also three values of coefficient of restitution were considered. A three inch and a ten inch free travel damper were considered. This amounted to increasing the boundaries or increasing the allowable η_M in the simulation. The ten inch free travel length was studied to investigate the effects of extended travel length only. No other system numbers such as damper system location, weight, volume, or vehicle aerodynamics and weight were modified to accommodate this change. Table III gives the basic range of damper parameters that were investigated.

TABLE II UNDAMPED TRAJECTORIES

Entry Velocity, V ft/sec	Entry Angle, θ deg	Initial Altitude, h_o ft	Entry Angle-of-Attack, α_i deg	Initial Angular Rate, $\dot{\alpha}_o$ rad/sec	Initial Dynamic Pressure, q_o lb/ft^2
21,800	90	192,000	155	2.4	6.1
21,800	90	192,000	138	1.8	6.1
21,800	90	192,000	109	1.2	6.1
21,800	90	192,000	57	.6	6.1
19,200	90	192,000	155	2.1	4.7
19,200	90	192,000	139	1.6	4.7
19,200	90	192,000	108	1.05	4.7
19,200	90	192,000	56	.5	4.7
15,000	16	232,000	180	.8	.4
15,000	16	232,000	72	.4	.4

TABLE III DAMPER PARAMETERS

Parameter	Symbol	Range
frequency	f	1,3,5 cps
% of critical damping	ζ	0,.5,1.0,2.0
coefficient of restitution	ϵ	0,.5,1.0
free travel length	η_M	$\pm$1.5in, $\pm$5in

2.3 Analog Computer Mechanization

The programming of the system equations was done using standard analog techniques. However the analog equipment used, Beckman 1132, has several features that facilitate solution of the two-body impact problem. The first of these is the complimentary integration scheme which was used to provide the new initial conditions after impact had occurred. Figure 3 indicates this mode of operation.

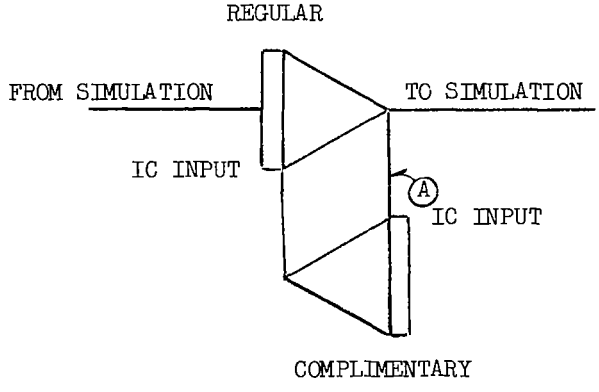

INTEGRATOR	MODE		
Regular	Compute	Hold	Initial Condition
Complimentary	Initial Condition	Hold	Compute

FIGURE 3. Complimentary Integration Scheme

From the mode identification, when the regular integrator is in compute C, the complimentary is in the IC mode and thus is just tracking the regular integrator. After the solution is stopped (at an impact) the regular integrator must receive an IC before integration proceeds. During this IC (on regular integrator) the complimentary integrator is in compute and its output is just the old value of the regular integrator output since it (the complimentary integrator) has only an IC input. Thus the output of the regular integrator has now been "wrapped around" and is now the IC for the next computation cycle. By inserting other components at A, the old output of the regular integrator can now be modified before it is used as an IC on the next cycle.

The other feature that was of use was the availability of multiple clocks. These clocks control the computation mode of groups of integrators. Separate clocks were used for the "η loop" and "α loop" integrators described in the following paragraphs.

The equations that were programmed were essentially Equations (10) and (11) of Section 2.1. Before proceeding in the usual analog fashion of solving for the highest derivative, the $M\eta^2$ term of the left-hand side of Equation (11) was examined and found to be at most less than 1.4% of the total inertia term. This term was dropped from the simulation since it was small and it also eliminated division by a variable in the programming of the equations. With this modification the equations are rewritten in analog fashion as Equations (35) and (36) below.

The impact representation, Equations (22) and (23), was programmed using the complimentary integrators as described previously. In addition to the equations there was the logic programming which ensured that problem solution, impacting, rate transferring, etc. occurred in the proper manner. The computer logic that is programmed to solve the system equations can be described briefly as follows.

- Initiate the solution to the two system differential equations for η and α

$$\ddot{\eta} = r\ddot{\alpha} + \dot{\alpha}^2\eta - \frac{F_N}{m_1} - \frac{F}{M} \tag{35}$$

$$\ddot{\alpha} = -\frac{M_A}{I} - \frac{M}{I}\eta\frac{F_A}{m_1} + \frac{rM}{I}\frac{F_N}{m_1} + \frac{rM}{I}\ddot{\eta} - \frac{2M}{I}\eta\dot{\eta}\dot{\alpha} \tag{36}$$

where $$I = I_1 + Mr^2 \tag{37}$$

- When $\eta = \pm \eta_M$; impact at a boundary has occurred and both solutions are stopped and held (the η loop and α loop integrators are on separate clocks).

- Change the variable rates $\dot{\eta}$, $\dot{\alpha}$, according to the impact equations

$$\dot{\eta}_a = -\epsilon\dot{\eta}_b \tag{38}$$

$$\dot{\alpha}_a = \dot{\alpha}_b - \frac{rM\,(1+\epsilon)}{I_1 + M\,(r^2 + \eta_M^2)}\,\dot{\eta}_b \tag{39}$$

- Examine $\dot{\eta}_a$

  if $\dot{\eta}_a \neq 0$; both loops are reinitialized with the new rates and the solutions continued to the next impact

  if $\dot{\eta}_a = 0$; only the α loop is reinitialized and restarted. Also the $\dot{\eta}$ and $\ddot{\eta}$ terms are removed from the simulation since the damper mass is at the wall and there is no relative velocity or acceleration. However, the $\ddot{\eta}$ amplifier is monitoring all the proper inputs and as soon as the sign of $\ddot{\eta}$ is opposite η, the η clock is started and the $\dot{\eta}$ and $\ddot{\eta}$ terms are replaced in the α loop integration. The solutions are continued until the next impact.

The analog patchboard wiring diagrams are included as Appendix I. The exponential atmosphere was generated as the solution to the following.

$$q = q_o e^{\beta V t} \tag{40}$$

This was, of course, only valid for portions of the atmosphere above 75,000 feet where the βV product is nearly constant. For the simulations that went deeper into the atmosphere, where the scale height is not constant, the value of q was generated with a function generator. Function generators were also used for generation of the aerodynamic coefficients.

Since the dynamic range on the analog is limited to a factor of about 200, the trajectory runs were limited in length. NASA/GSFC provided the basic trajectories without the damper. The trajectories in this study were begun at the first zero crossing of angle-of-attack in the NASA provided trajectories. For the 21,800 ft/sec and 19,200 ft/sec entries this was at an altitude of about 192,000 with a q_o of 6.1 and 4.7 lb/ft^2 respectively. With the aforementioned range of about 200 these trajectories were then q limited and were scaled to a maximum value of q = 1000 lb/ft^2. The altitude at which this occurs is about 85,000 feet.

The grazing entry at 15,000 ft/sec however has its first angle-of-attack zero crossing at 232,000 feet and a much lower q_o namely .4 lb/ft^2. To accurately simulate this trajectory, the problem had to be rescaled and thus was q limited at 100 lb/ft^2. This occurred at an altitude of 115,000 ft. Since the grazing entry was not the primary trajectory, only this range was examined. The 21,800 ft/sec and 19,200 ft/sec entries were carried to deeper altitudes. To do this, however, required significant changes to the programming. Because the frequency was higher, 3-5 cps, the problem was time scaled by a factor of 10. Since q would increase to about 5000 psf, amplitude scaling was also required. The βV term in the generation of q, Equation (40), is no longer constant below approximately 75,000 feet thus the generation of q was done with a function generator. These "deeper" entry trajectories were run from about 132,000 feet down to about 45,000 feet and thus overlapped the original set. To match the previous set, various initial angular rates on angle-of-attack were run with the damper mass in different positions. The damper mass initial position had little effect on angle-of-attack envelope so the deeper entry trajectories were matched to the originals by matching angular rates at a common altitude.

Because there were numerous changes involved in considering the various trajectories, the studies were performed in the order just described, that is

21,800 ft/sec entry; 192,000 ft down to 85,000 ft; 3" and 10" free travel length
19,200 ft/sec entry; 192,000 ft down to 85,000 ft; 3" and 10" free travel length
15,000 ft/sec entry; 232,000 ft down to 115,000 ft;3" and 10" free travel length
21,800 ft/sec entry; 132,000 ft down to 45,000 ft; 3" free travel length
19,200 ft/sec entry; 132,000 ft down to 45,000 ft; 3" free travel length

In the deeper entry trajectories only the 3" free travel length damper was considered, and only those 3" free travel length dampers that had shown promise in the original study were continued in the deeper entry portion of the study.

2.4 Parametric Study Results

For comparison in evaluating the performance of the damper system on the angle-of-attack oscillations, data on the undamped trajectories (with no damper) are presented in Figures 4-7. Figures 4-6 give the angle-of-attack entries for the ten entry trajectories considered. Also shown are the dynamic pressure, q, and the frequency of the angle-of-attack oscillations. The frequency is calculated by taking the time between successive angle-of-attack zero crossings as a half period. The energy associated with the rotational mode of motion increases with entry, thus it is desirable to reduce the amplitude as early as possible. The frequency plotted is that taken from the undamped trajectory. The additional mass due to the damper tends to decrease this frequency, also the initial angular rate imparted to the system alters the frequency. Both of these effects cause less than a 10% change in frequency.

The problem is not one of pure rotation, however. A closer examination of all the terms in Equations (10) and (11) shows that the aerodynamic normal force F_N is very large. This force is large enough to produce lateral c.g. displacements of approximately two feet at the high initial rates. Figure 7 shows the angle-of-attack altitude history for the 21,800 ft/sec entry at the high initial angular rate of $\dot{\alpha}_o = 2.4$ rad/sec. Below it is the aerodynamic induced acceleration normal to the entry vehicle longitudinal axis (and in the η direction). Also shown is the normal acceleration of the slot location ($r = .917$ ft) due to rotation only. The normal acceleration seen at the slot location is about 2/3 normal force induced and about 1/3 rotationally induced. If the motion is assumed periodic for one cycle and displacement is calculated as (at 100,000 ft),

$$\text{Displ} = \frac{\text{Accel}}{\omega^2} = \frac{A_N + r\ddot{\alpha}}{\omega^2} = \frac{220 + .917 \times 100}{(2\pi)^2(2)^2} = 2 \text{ ft}$$

Thus the slot location on the entry vehicle undergoes a periodic inertial displacement of the order of 2 feet in the η direction. Since the damper system is to utilize the relative motion between damper mass and entry vehicle it is necessary that the damper mass have as much free travel as possible. This conclusion was borne out as the 10" free travel damper was more efficient in every comparable case.

To measure damper effectiveness, angle-of-attack envelopes for trajectories both with and without the damper were compared. From this data two sets of damper parameters were obtained. One set is for the 3" free travel case and the other is for the 10" free travel case. These were selected as the dampers displaying the maximum effectiveness for the case of $\alpha_i = 155°$. These are not necessarily the best for the lower initial angle-of-attack cases. The charactersitics of the dampers selected are

3" free travel length	10" free travel length
$f = 1$ cps	$f = 1$ cps
$\zeta = 2.0$	$\zeta = .5$
$\epsilon \approx 1.0$	$\epsilon = .5$

The angle-of-attack envelopes for these two dampers for the ten entry trajectories are shown in Figures 8-17. Figures 18 and 19 show the damper mass relative motion, η, and angle-of-attack, α, for a typical case for various values of coefficient of restitution, ϵ. The detailed results of the computer study are presented in tabular form in Appendix II.

In general the viscous damping was more effective than impacting at the boundary. This is due, in large part, to the high ratio of the inertial motion of the damper slot to the damper relative free travel motion. If this ratio is high then a relatively large amount of time is spent against the stops doing no work. However if the damper mass rebounds (and thus does not dissipate energy at impact), energy is dissipated through viscous effects during the relative motion.

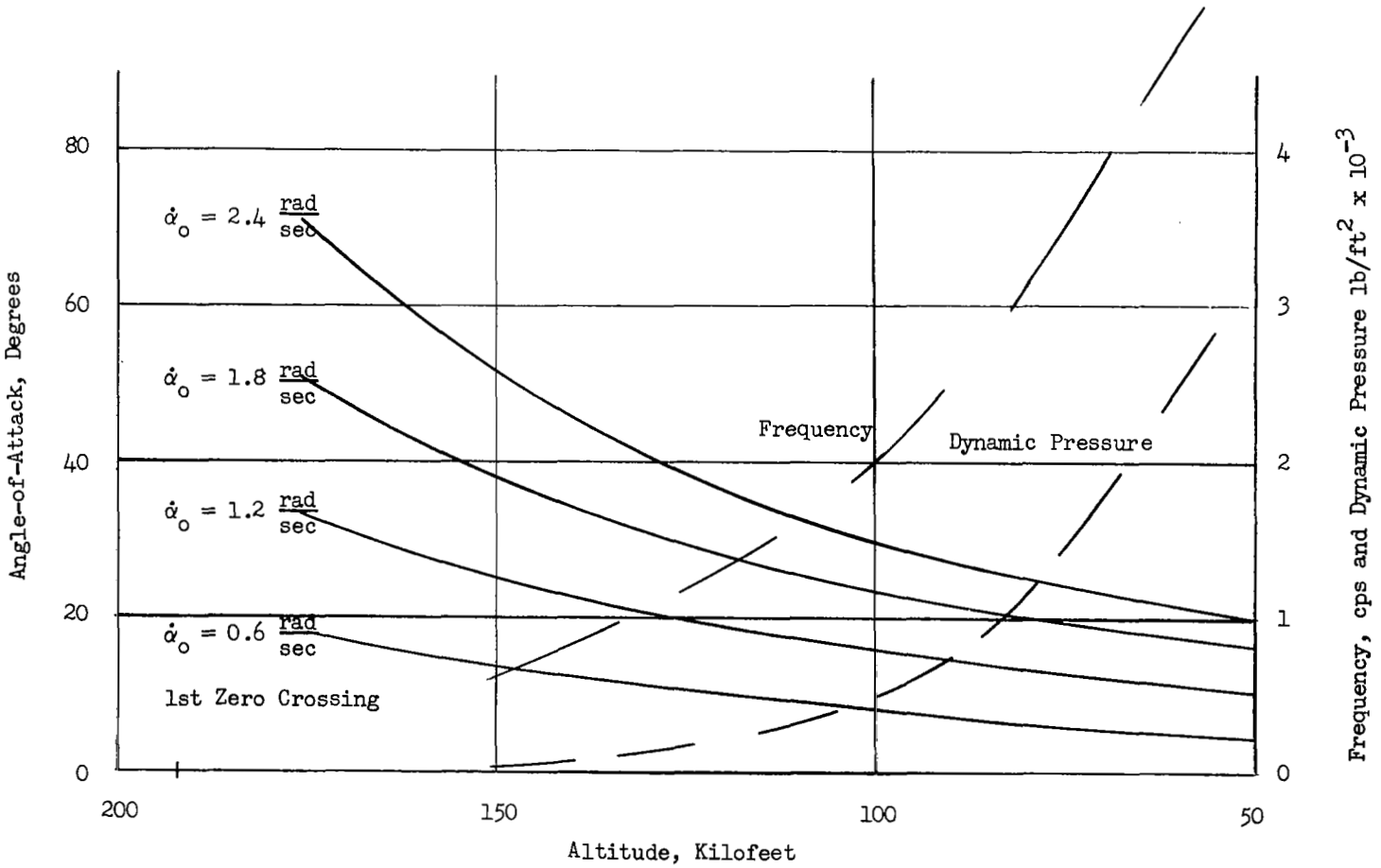

FIGURE 4 Angle-of-Attack Envelope - versus Altitude
Undamped Trajectories - V=21,800 ft/sec., θ=90 deg.

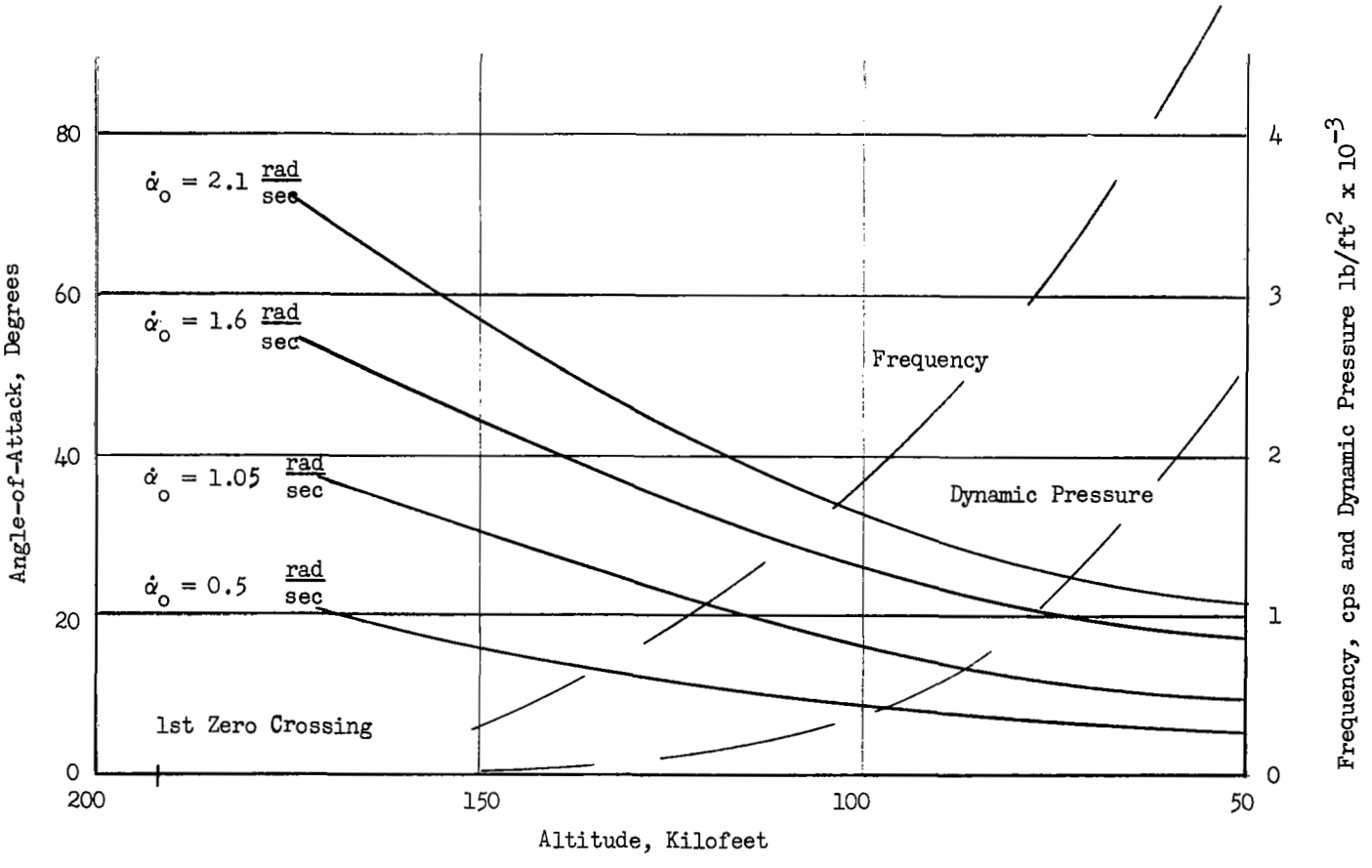

FIGURE 5 Angle-of-Attack Envelope - versus Altitude
Undamped Trajectories, V=19,200 ft/sec., θ=90 deg.

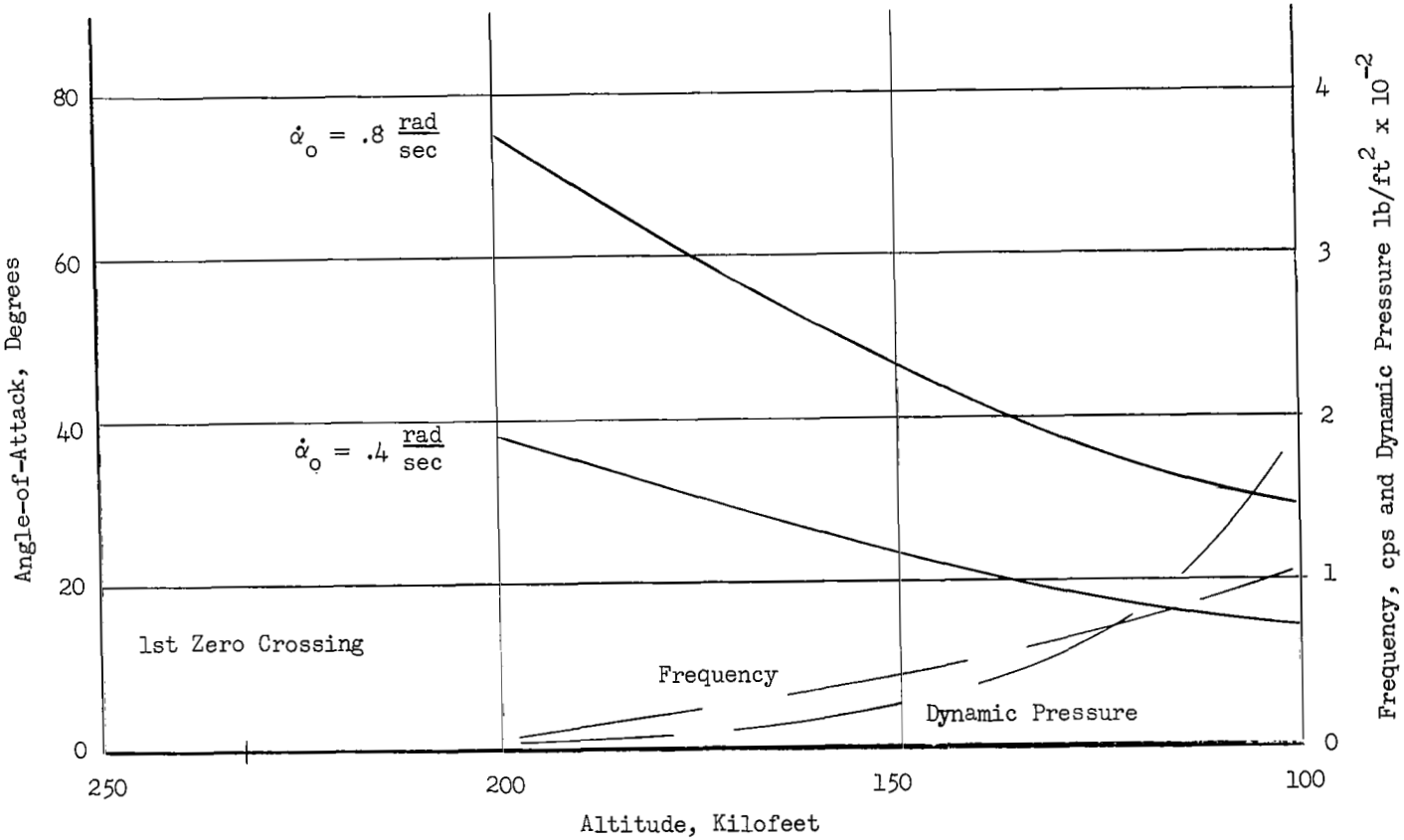

FIGURE 6 Angle-of-Attack Envelope - versus Altitude
Undamped Trajectories, V=15,000 ft/sec., θ=16 deg.

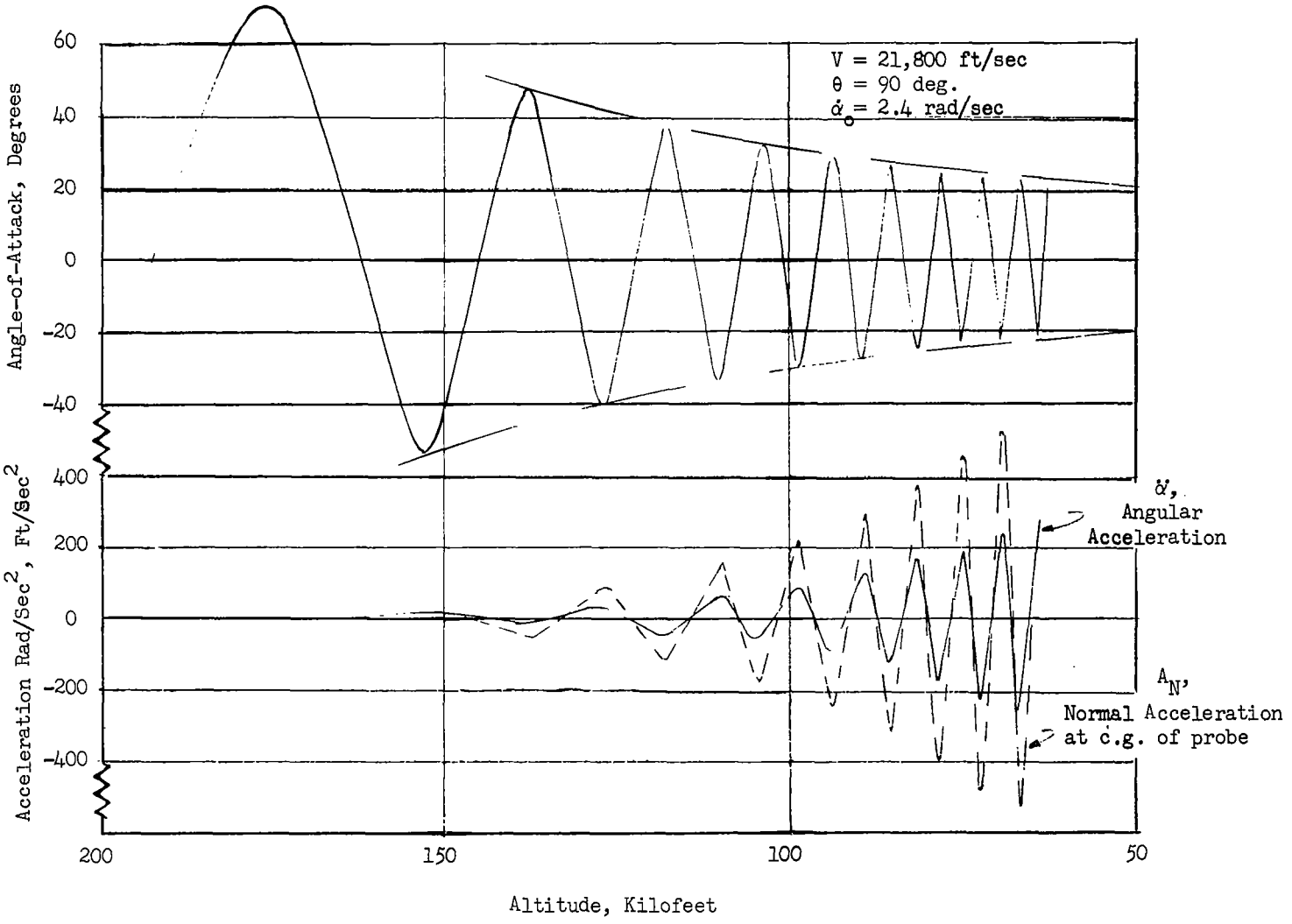

FIGURE 7 Angle-of-Attack and Normal Acceleration versus Altitude for Undamped Trajectories

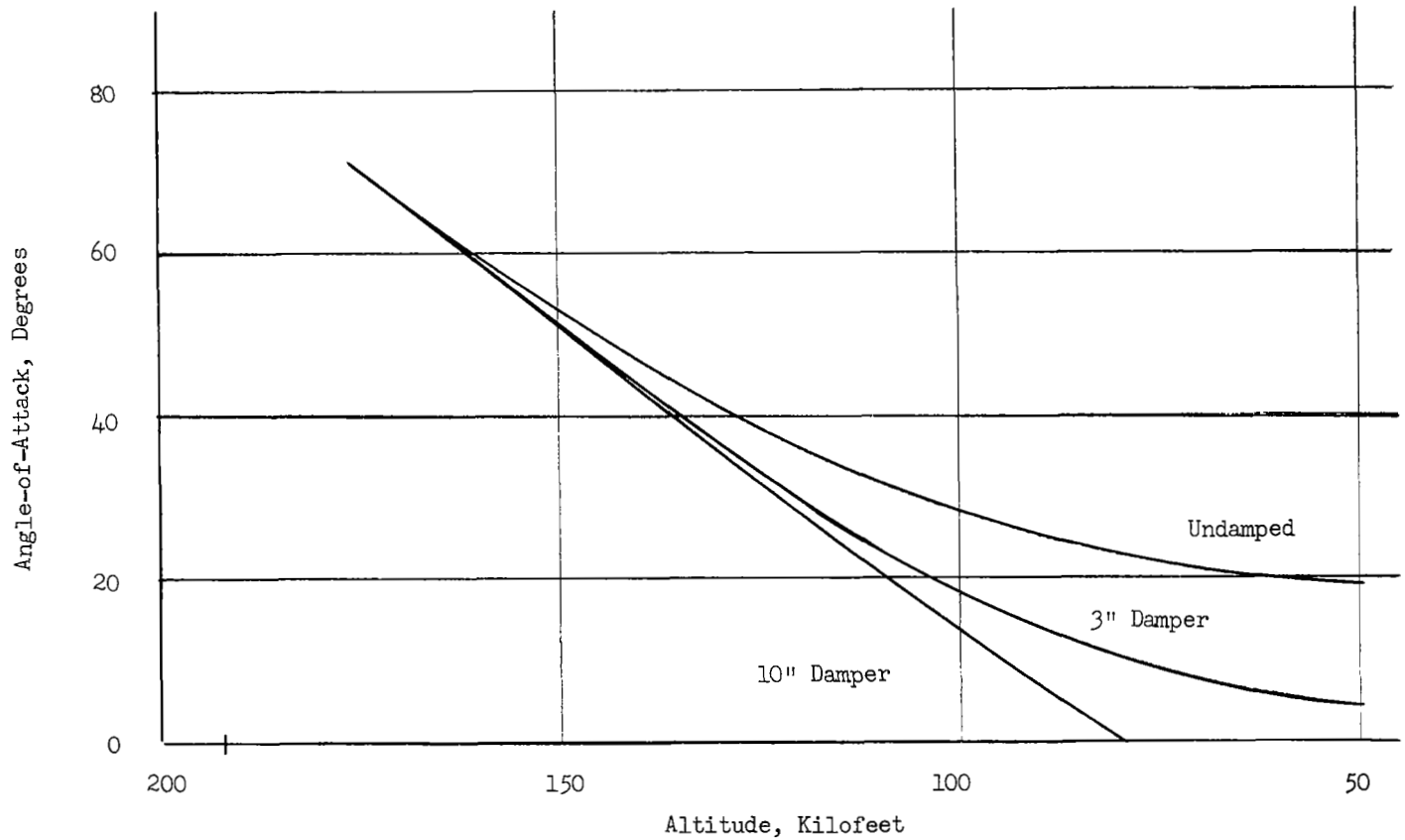

FIGURE 8 Angle-of-Attack, V=21,800 ft/sec., $\dot{\alpha}_o$=2.4 r/sec., θ=90 deg.

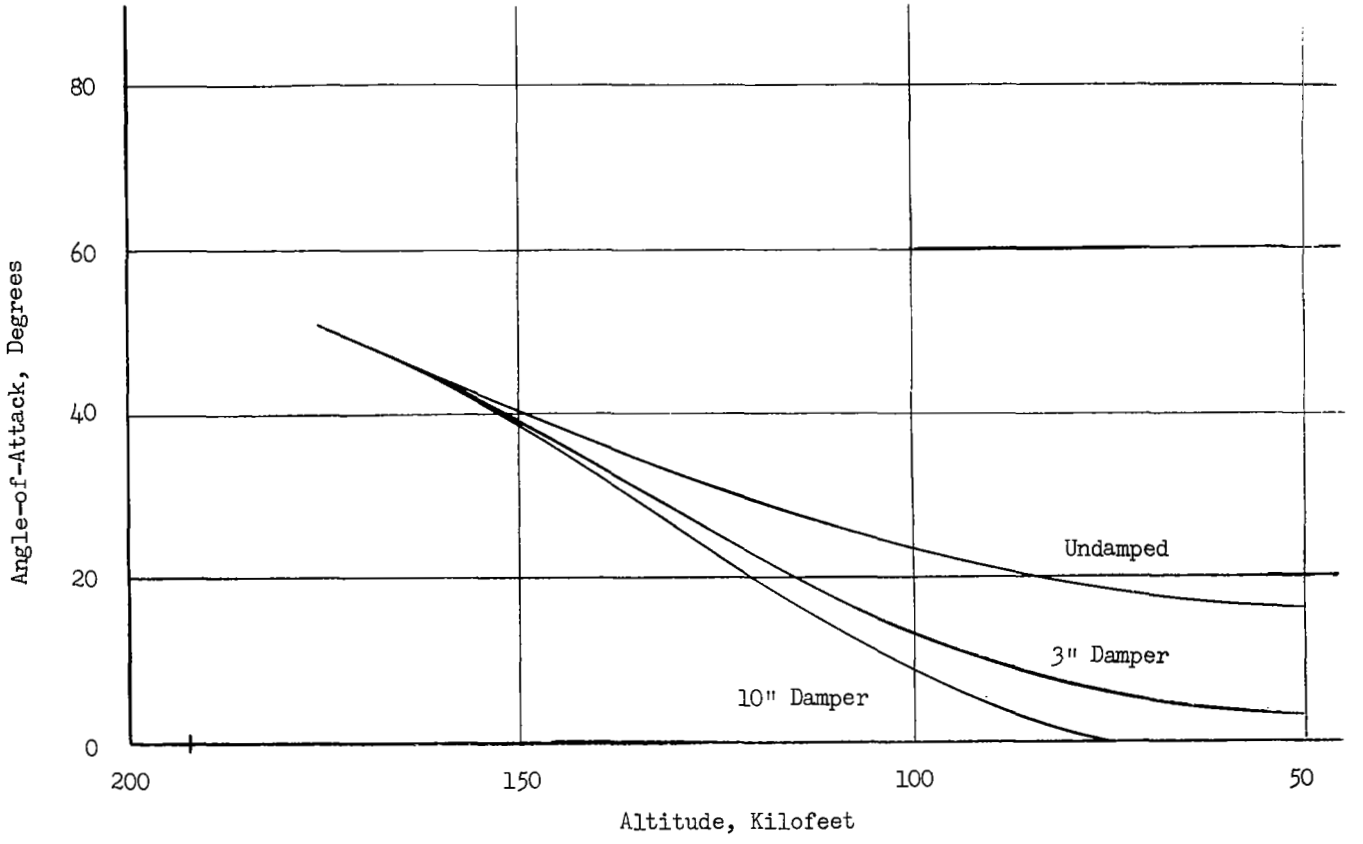

FIGURE 9 Angle-of-Attack, V=21,800 ft/sec., $\dot{\alpha}_o$=1.8 r/sec., θ=90 deg.

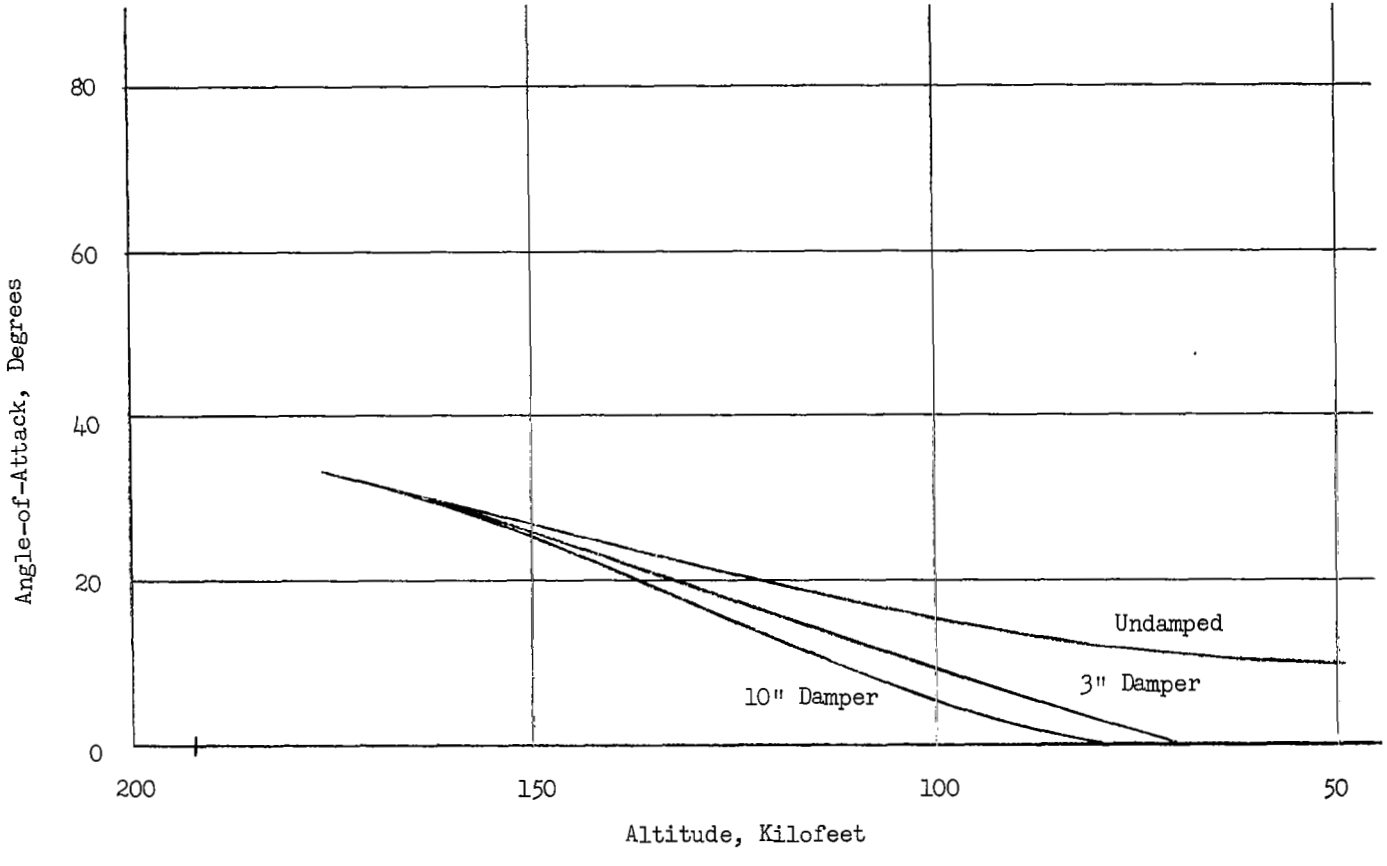

FIGURE 10 Angle-of-Attack, V=21,800 ft/sec., $\dot{\alpha}_o$=1.2 r/sec., θ=90 deg.

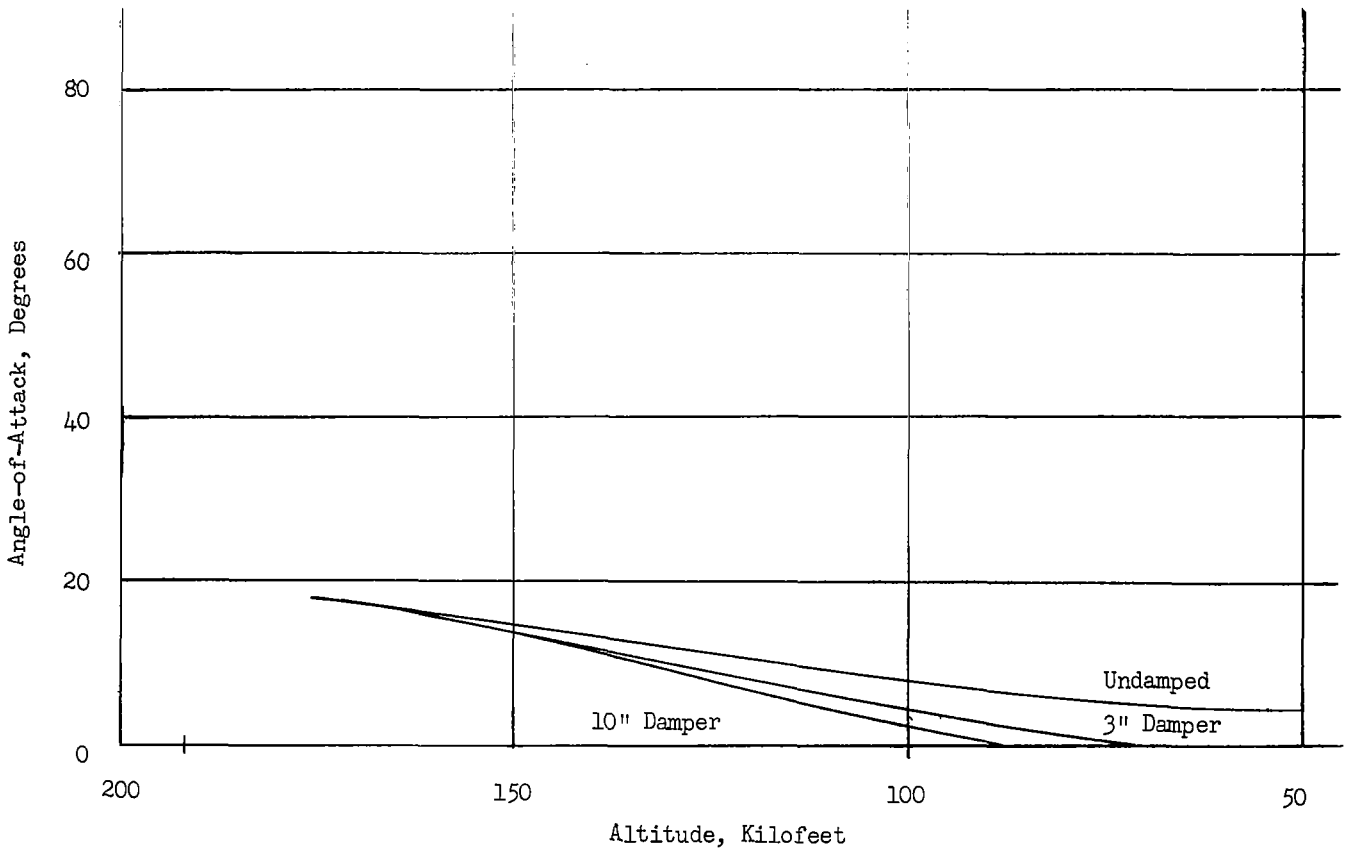

FIGURE 11 Angle-of-Attack, V=21,800 ft/sec., $\dot{\alpha}_o$ = .6 r/sec., θ=90 deg.

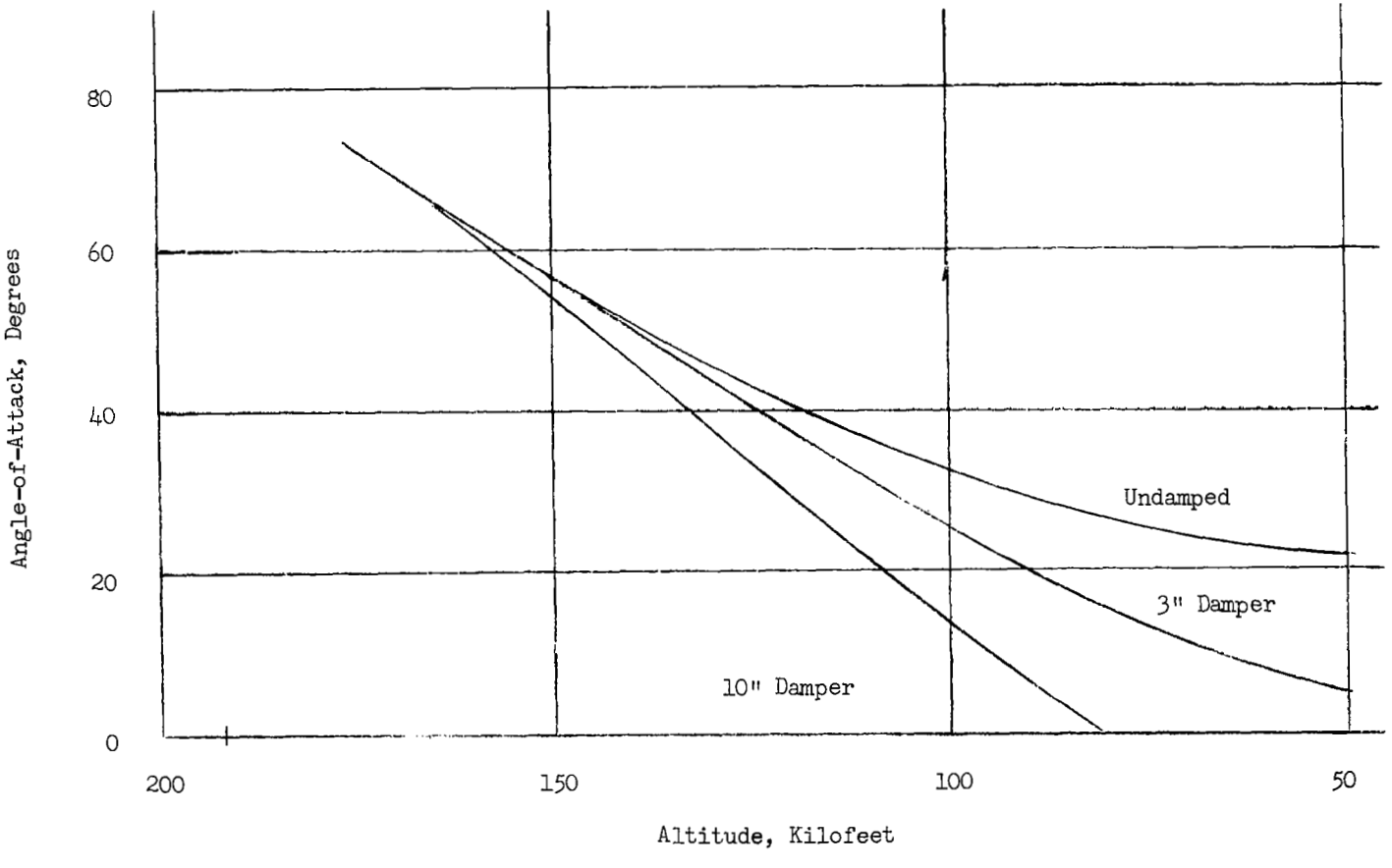

FIGURE 12 Angle-of-Attack, V=19,200 ft/sec,, $\dot{\alpha}_o$=2.1 r/sec., θ=90 deg.

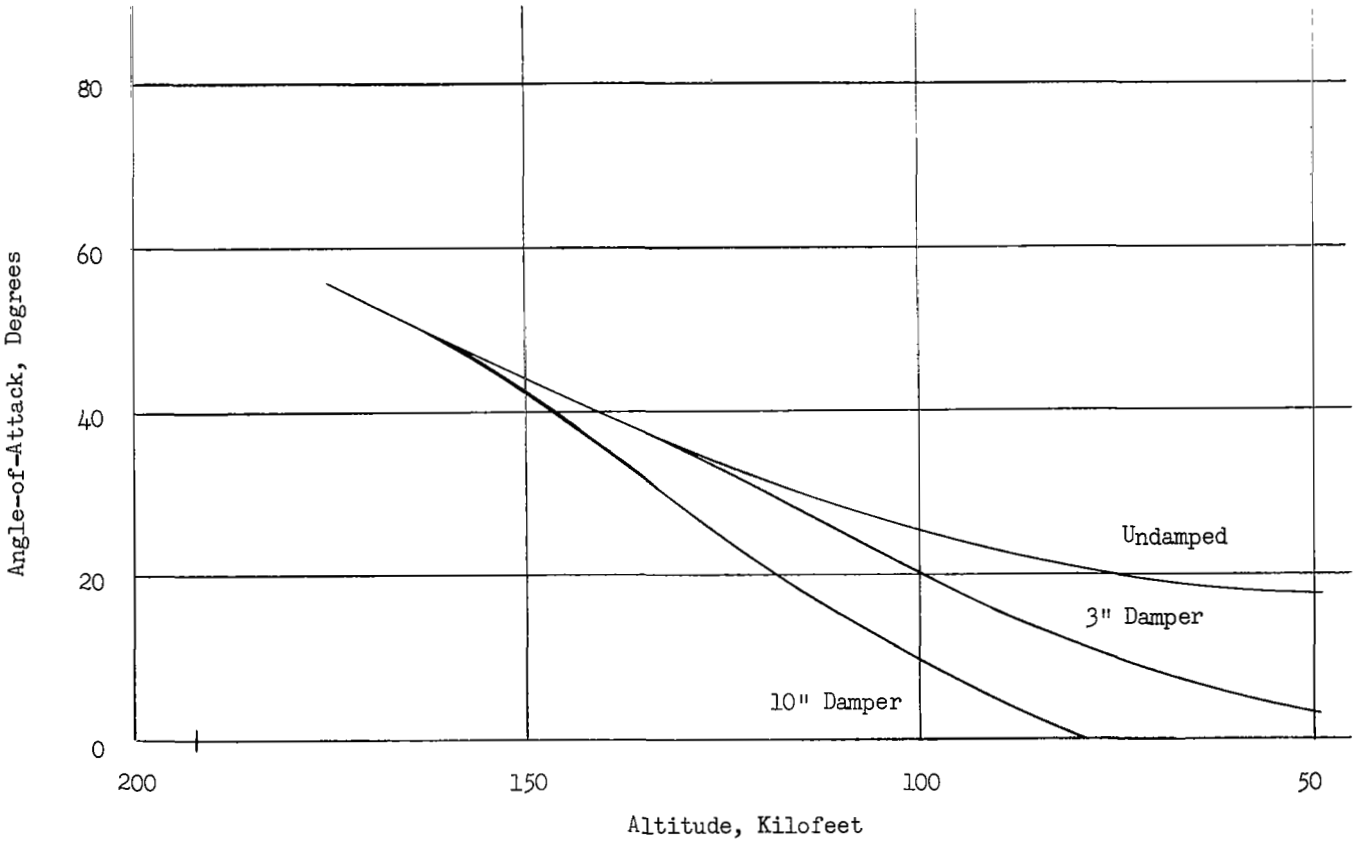

FIGURE 13 Angle-of-Attack, V=19,200 ft/sec., $\dot{\alpha}_o$=1.6 r/sec., θ=90 deg.

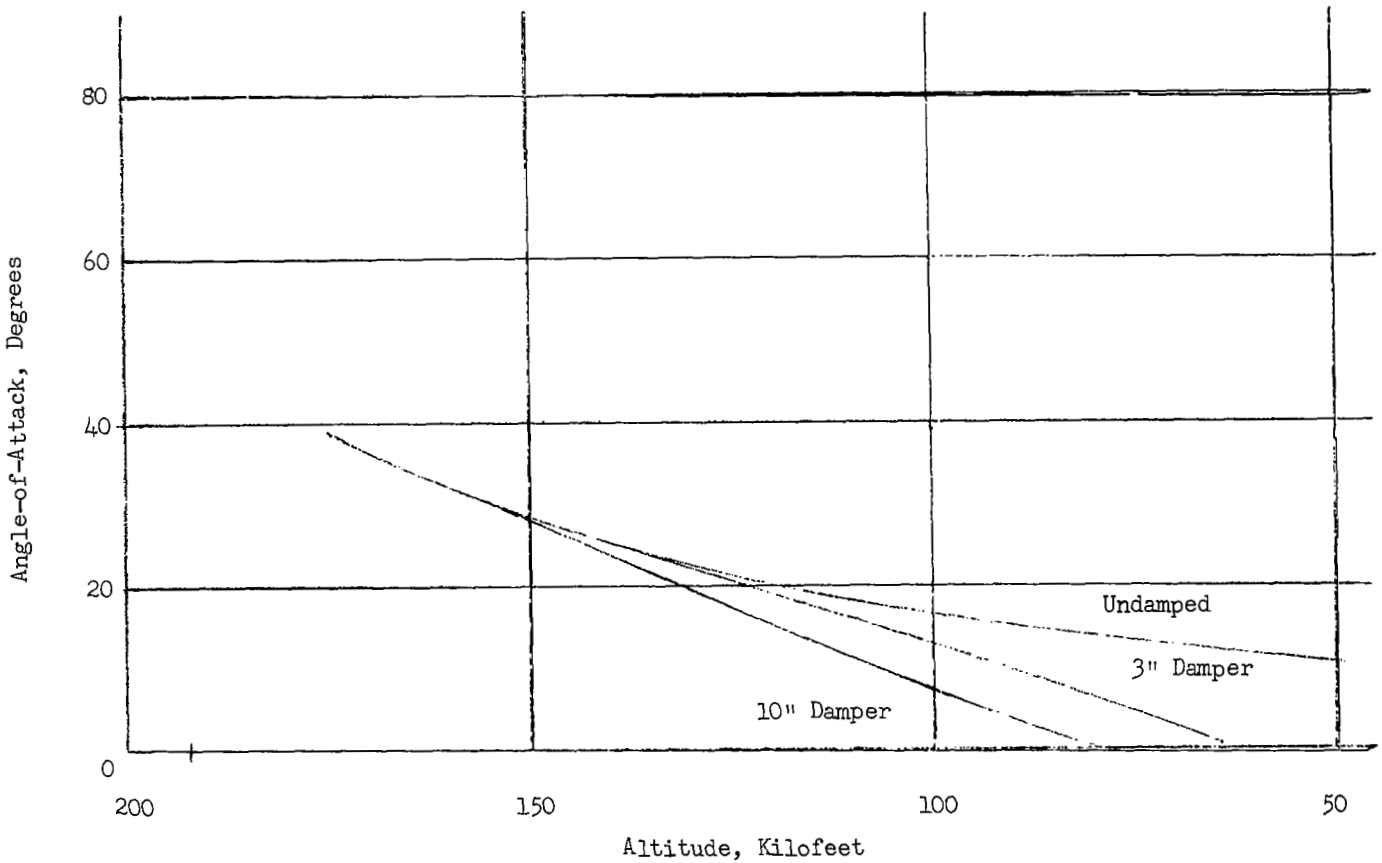

FIGURE 14 Angle-of-Attack, V=19,200 ft/sec., $\dot{\alpha}_o$=1.05 r/sec., θ=90 deg.

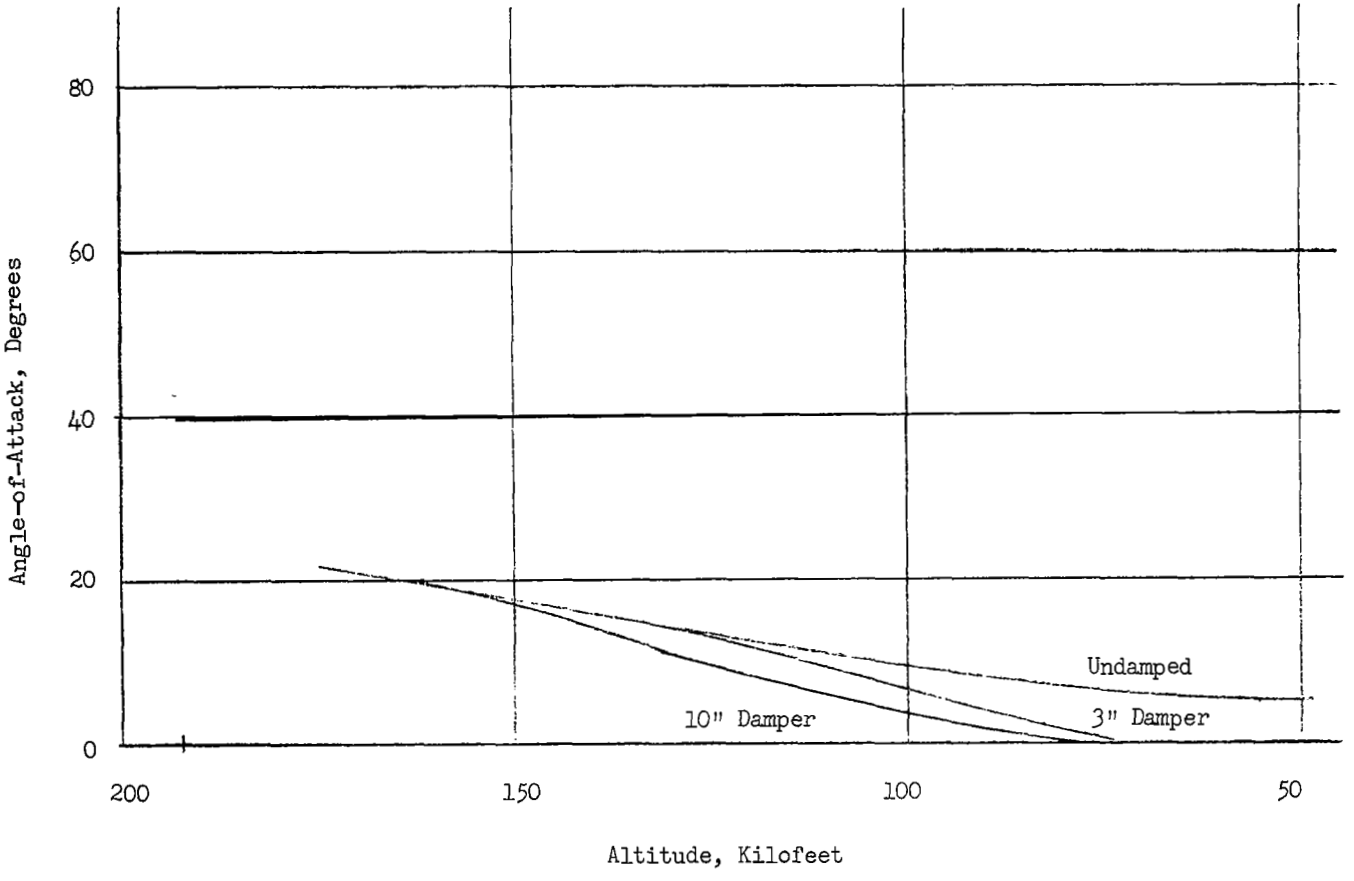

FIGURE 15 Angle-of-Attack, V=19,200 ft/sec., $\dot{\alpha}_o$=.5 r/sec., θ=90 deg.

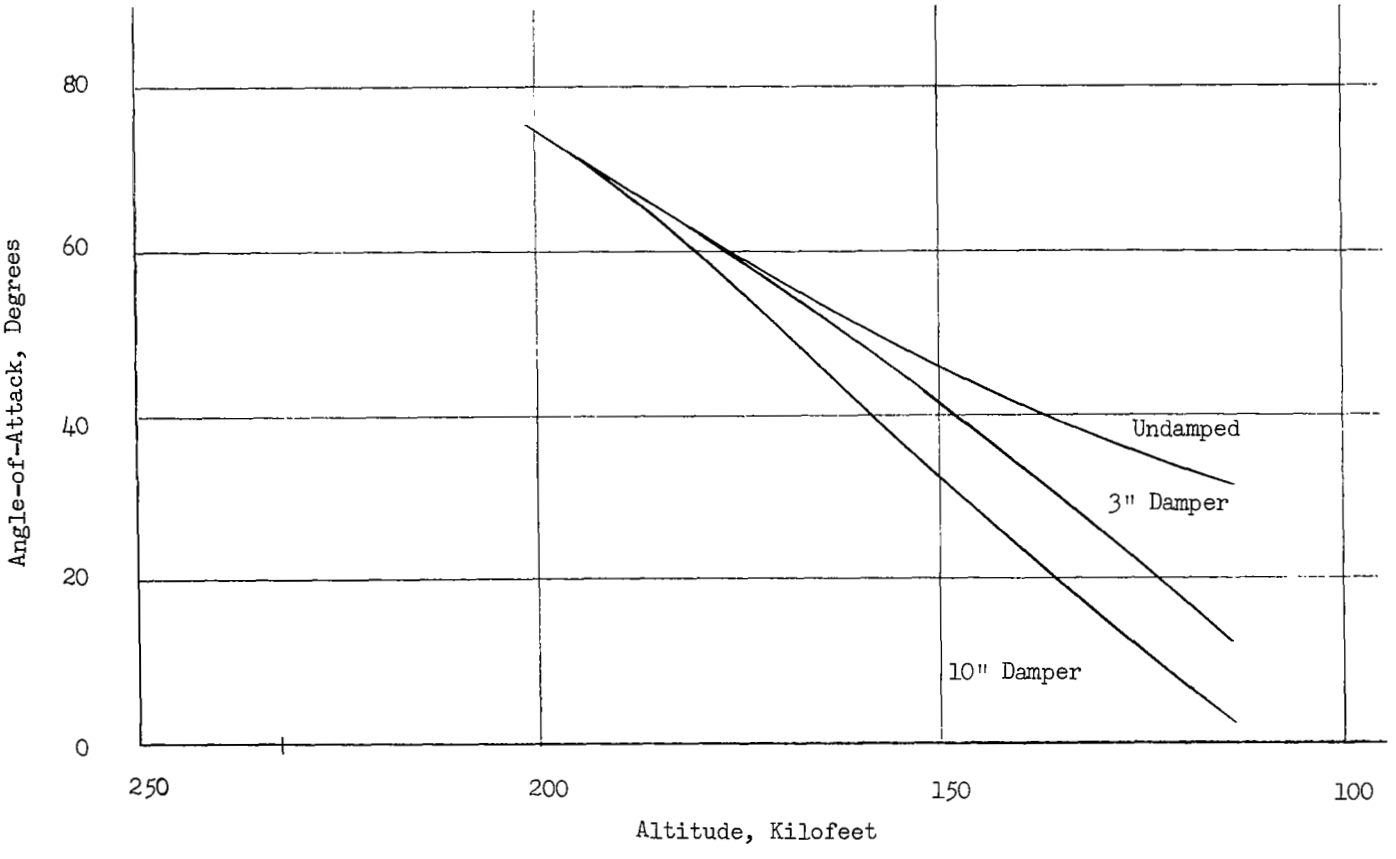

FIGURE 16 Angle-of-Attack, V=15,000 ft/sec., $\dot{\alpha}_o$=.8 r/sec., θ=16 deg.

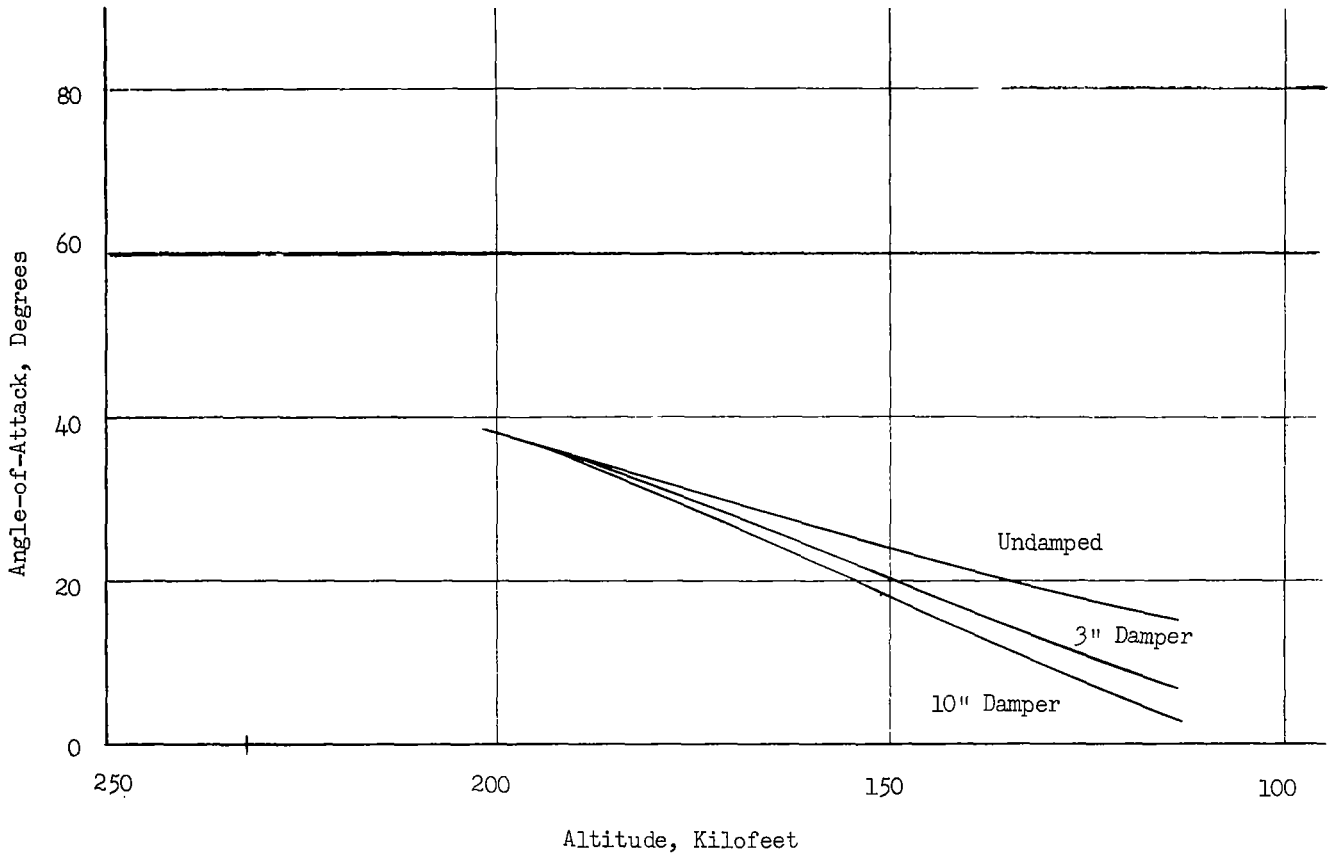

FIGURE 17 Angle-of-Attack, V=15,000 ft/sec., $\dot{\alpha}_o$=.4 r/sec., θ=16 deg.

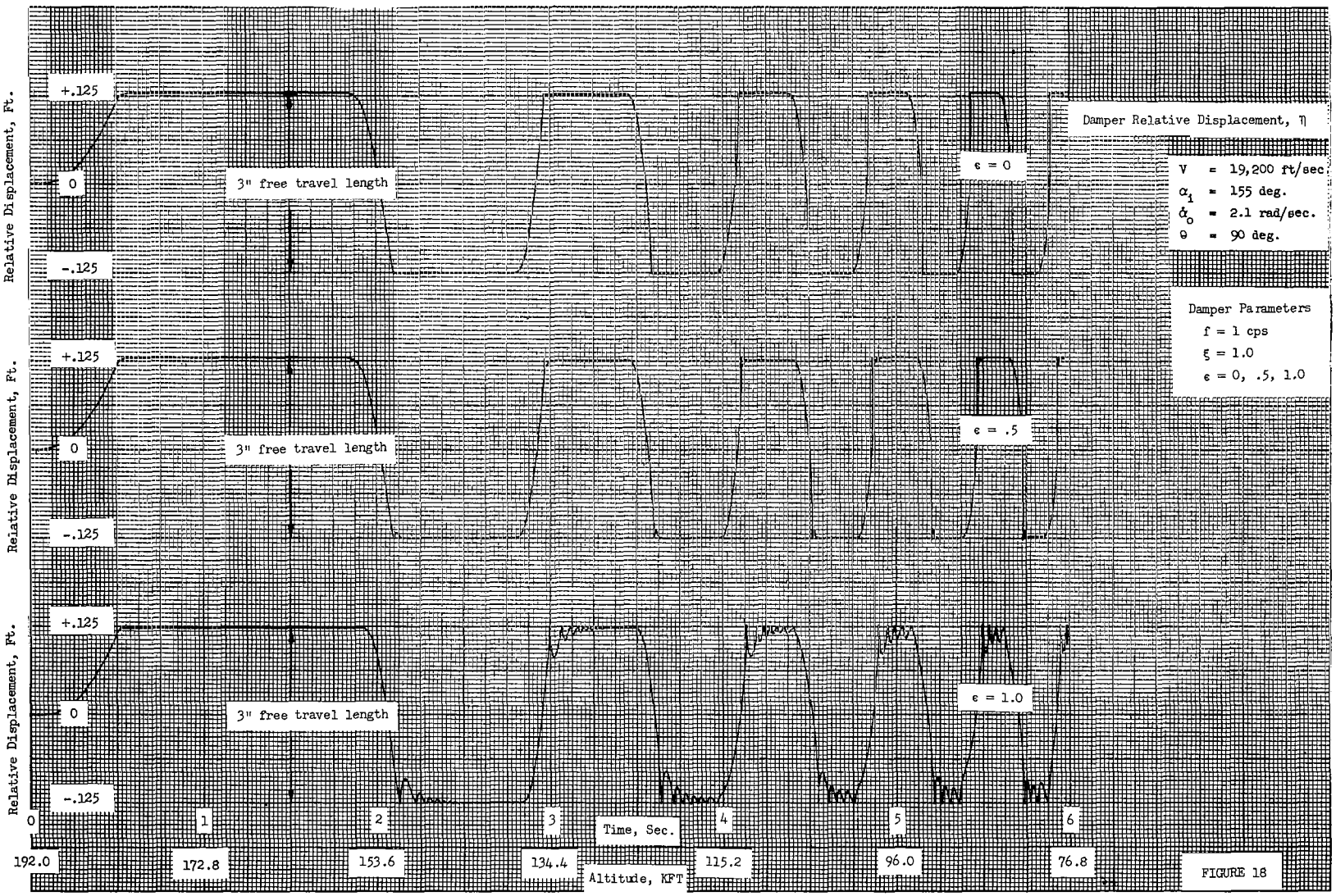
Relative Displacement, Ft.
+.125
0
-.125
3" free travel length
ε = 0
Damper Relative Displacement, η
V = 19,200 ft/sec
α_i = 155 deg.
$\dot{\alpha}_o$ = 2.1 rad/sec.
θ = 90 deg.
Damper Parameters
f = 1 cps
ξ = 1.0
ε = 0, .5, 1.0
ε = .5
ε = 1.0
0
1
2
3
4
5
6
Time, Sec.
192.0
172.8
153.6
134.4
115.2
96.0
76.8
Altitude, KFT

FIGURE 18

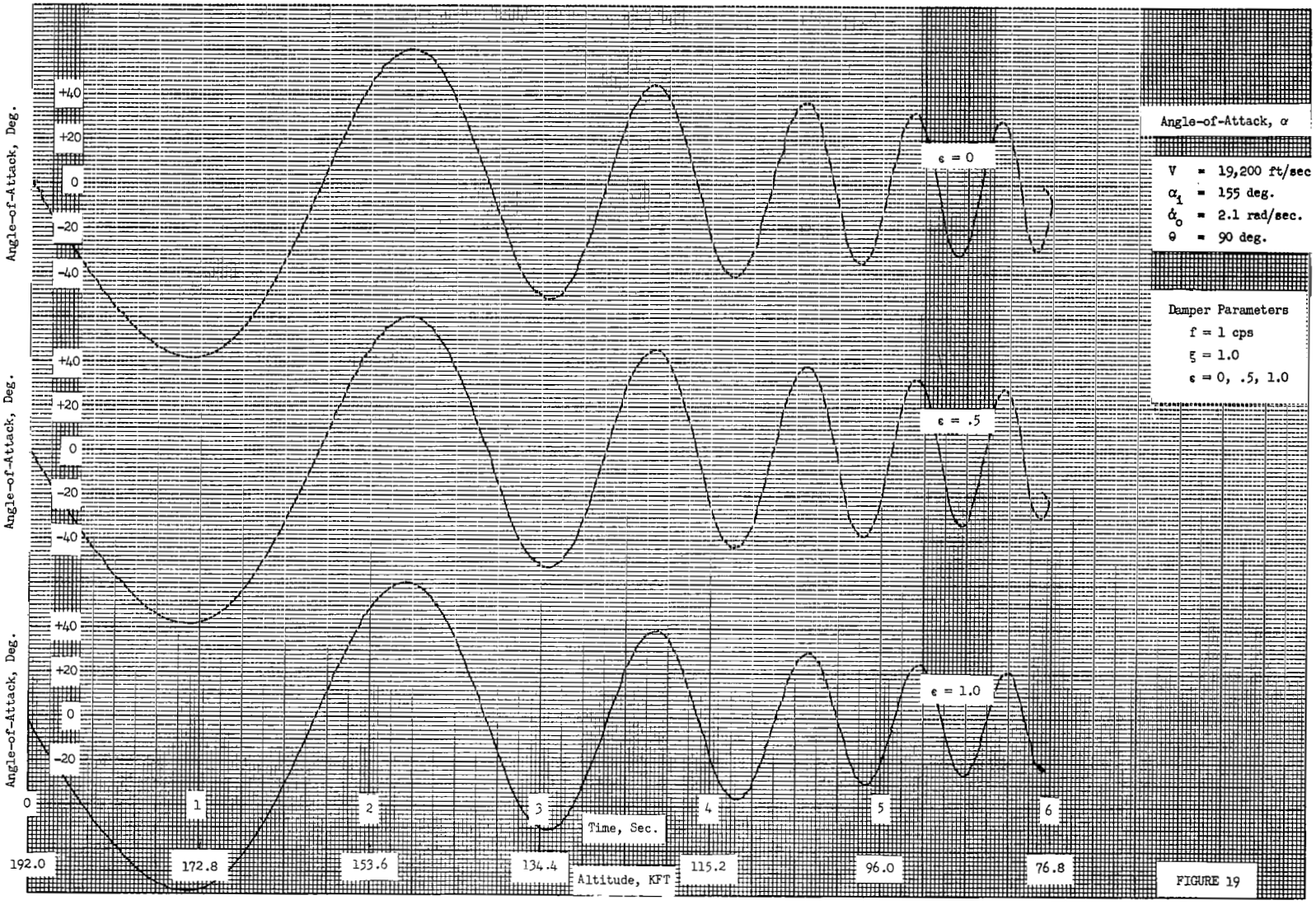
Angle-of-Attack, Deg.
+40
+20
0
-20
-40
Angle-of-Attack, Deg.
Angle-of-Attack, Deg.
0
1
2
3
4
5
6
Time, Sec.
192.0
172.8
153.6
134.4
115.2
96.0
76.8
Altitude, KFT
ε = 0
ε = .5
ε = 1.0
Angle-of-Attack, α
V = 19,200 ft/sec
α_i = 155 deg.
α̇_o = 2.1 rad/sec.
θ = 90 deg.
Damper Parameters
f = 1 cps
ξ = 1.0
ε = 0, .5, 1.0

FIGURE 19

3. DAMPER DESIGN

3.1 Design Criteria

The criteria that results from the parametric study can be briefly stated. For a damper with only three (3) inches of free travel length the following parameter values were most effective.

$f = 1$ cps
$\zeta = 2$
$\epsilon = 1.0$

For the damper with ten (10) inches of free travel length the following parametric values were most effective.

$f = 1$ cps
$\zeta = .5$
$\epsilon = .5$

Analytically, the above parameters demonstrate the best set of parameters in reducing angle-of-attack for the system studied. It is well to recall the major assumptions of the study, namely - planar motion only was considered, only a fixed vehicle mass and one damper mass were considered, and a rather simple concept of a linear spring and damping proportional to velocity were considered. In addition, the phenomenon at impact on the boundary is simply represented by using a coefficient of restitution.

One of the design constraints placed on the probe is the sterilization requirement. The sterilization cycle requires a 36 hour soak at 145°C. The probe on the other hand is to be thermally controlled at -12°C during its approach to and descent towards the planet. The damper system will be exposed to temperatures ranging from 145°C to -12°C and must be able to operate at about -12°C.

As originally required the damper system was to occupy about 60 cubic inches, weight about 6 pounds, and be located approximately 11 inches to the rear of the c.g. (Reference 1). However, during the study the large (10") free travel length was introduced into the analysis. With no other modifications, the 10" free travel damper would not fit at the same location in the same probe. However the analyses on the 10" free travel length damper were carried out only to point out the effect of the free travel parameter. Even though the study was planar, the development of the concept was such that the dampers' effectiveness was omnidirectional.

3.2 Design Concept

The damper concepts are shown in Figures 20 and 21. Briefly the damper system consists of a sprung mass immersed in a cannister filled with a viscous fluid to provide damping.

The suspension system is such that the spring rate is roughly equivalent in any direction and thus the mass will always oscillate in the excitation plane. In the 10" free travel length damper two spiral springs are needed so that the base moments are negated and no roll acceleration is imparted to the entry probe. The two coils of the spring should give fairly omnidirectional stiffness. The springs in the 3" free travel length damper will collapse in compression and be contained within the slot without damage. The suspension system is slightly nonlinear with displacement amplitude.

Impacting at the boundary with various coefficients of restitution is handled by putting rubber pads around the tungsten mass. Although a coefficient of restitution of unity cannot be attained, anything up to .90 can be attained with rubber. Rubber and the silicone fluid are compatible at the temperature extremes expected. The thermal expansion of the silicone fluid is high, thus a bellows accumulator was incorporated to handle the increased volume during the sterilization cycle.

The damping is provided by mass traveling through and shearing the viscous fluid. The actual damping force was calculated using laminar flow theory. Stiction will be minimal due to the high frequency vibration environment. The coefficients of kinematic viscosity required are in the 1000 to 10,000 centistoke range. The Dow Corning 200 series fluids are available in the 1 to 10^6 centistoke range with other properties (density, and thermal expansion) the same.

In the attainment of the study objectives, namely, establishing design criteria and providing a conceptual design satisfying those criteria it is worthwhile to note other considerations. Although the study was planar and the design concept generated was to be omnidirectional, further analytical studies should be performed to examine the true six degree of freedom motion of the entry vehicle. The supporting calculations in the following section are only detailed enough to ensure availability, sizing, strength, and compatibility of existing materials. Ground testing will be necessary to evaluate the performance of the system and to establish the accuracy of the supporting design analysis.

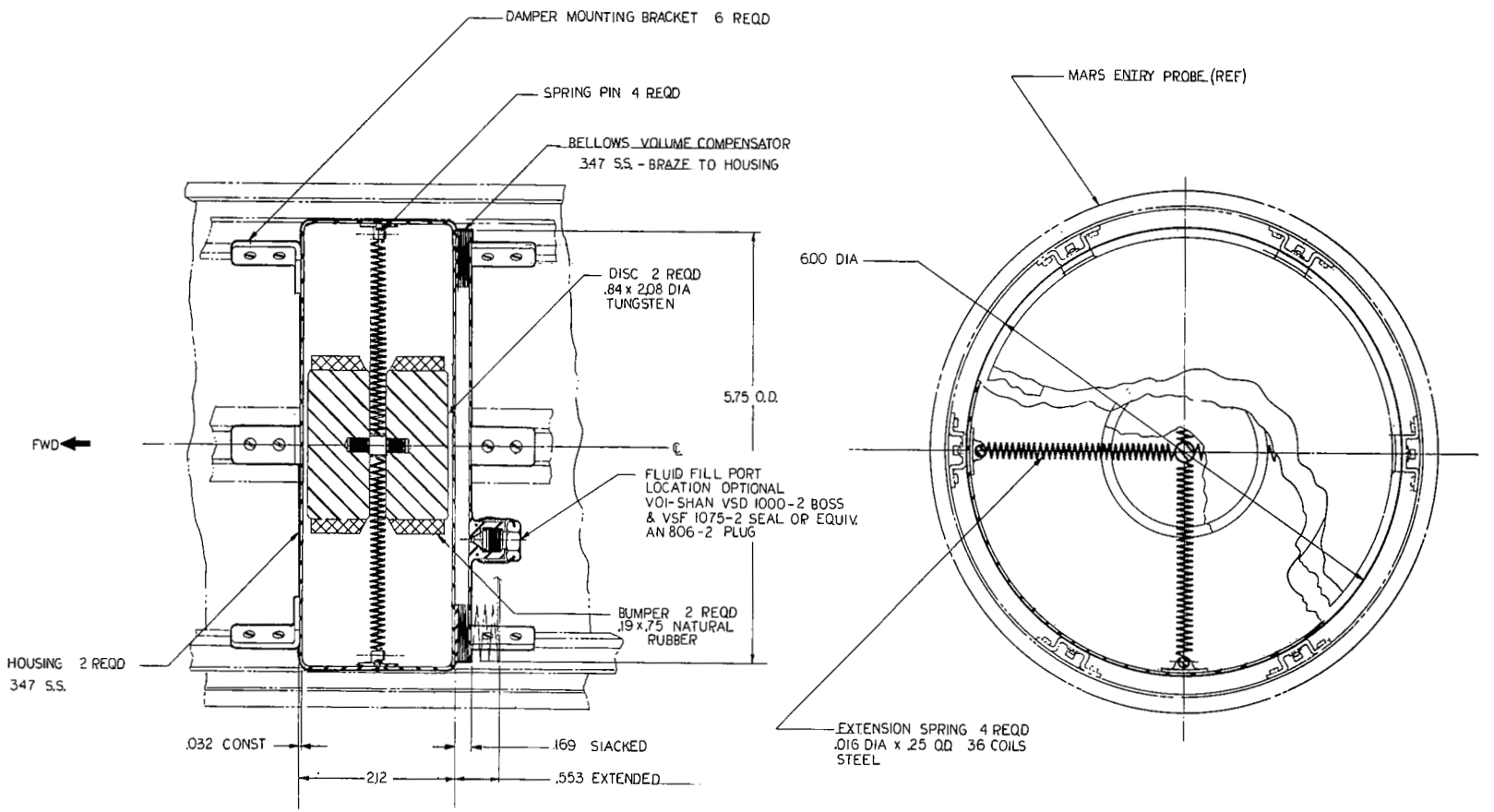

FIGURE 20 Passive damper, 3.00 free travel length.

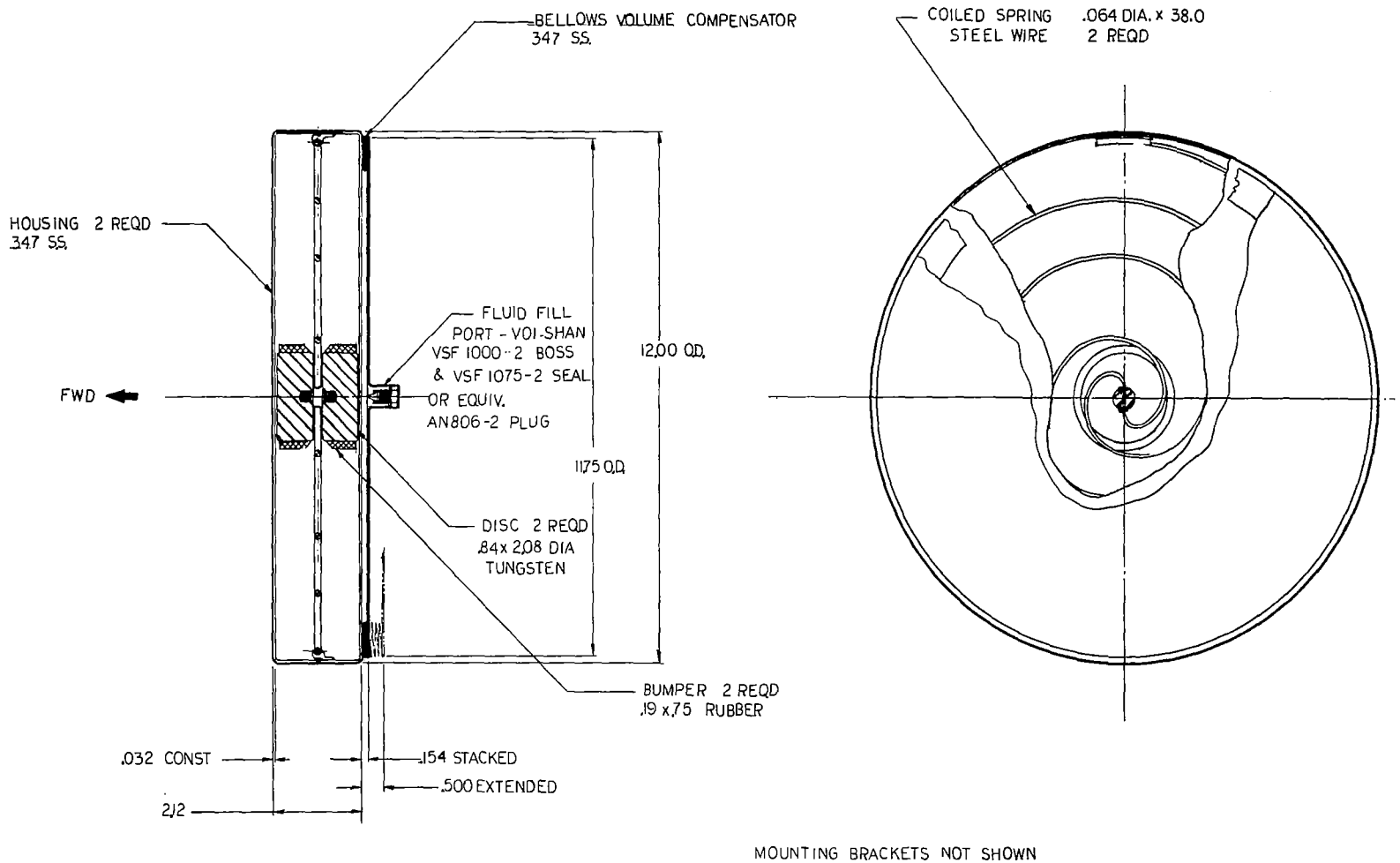

FIGURE 21 Passive damper, 10.00 free travel length.

3.3 Supporting Calculations

3.3.1 3 Inch Free Travel Length Damper

The damper consists of a four pound mass immersed in a silicone damping fluid and suspended by four coil extension springs spaced at 90° intervals. The mass is in the form of two tungsten discs separated by the spring mounting post. Natural rubber bumpers are attached to the discs and are shaped to guide the spring into the space between the discs. The axial g loading will cause the springs to sag but they will be scooped up into the damper slot to prevent damage. Due to the increase of 16% in fluid volume encountered during the sterilization cycle, a bellows accumulator is utilized in the design. The accumulator is brazed to the main damper housing. A fill port using a Voi-Shan boss and conical seal insures zero leakage and allows for opening of the damper for fluid replacement. The bellows and housing are made of 347 stainless steel.

Extension Spring Design

The extension spring is to be designed with a spring rate of 5 lb/ft. This corresponds to a natural frequency of 1 cps. Assume that the two springs in parallel give the desired rate of 5 lb/ft = .408 lb/in. Thus each spring must have a rate of .204 lb/in. Also assume the unstretched length of the spring and end connections to be 2 inches. Thus the maximum extended length of any of the 4 springs is 3 inches. Note that with this size only one spring at a time will be forced into compression. In the center position each spring will be in tension. At full deflection, 3 in., the load, P, in the spring will be

$$P = .204 \frac{lb}{in} \times 3 \text{ in.} = .612 \text{ lbs}$$

Using "MECHANICAL SPRINGS" by A. M. Wahl, pg. 78, a spring of music wire and the following properties is suitable.

d = .016 in wire diameter
D = .25 in coil diameter
spring rate per coil = 7.37 lb/in
load @ 100,000 psi corrected stress = .626 lbs

The number of coils, N, needed to give the desired spring is then (for springs in series)

$$N \times \frac{1}{7.37} = \frac{1}{.204} \quad \text{or } N = 36 \text{ coils}$$

The stacked length of the coils is 36 x .016 in = .58 in which leaves room for end loops. The critical buckling deflection is only about .1 in (WAHL page 69). The spring will buckle and thus not contribute to the total spring rate. The variation in spring rate (K_T) is then (see sketch).

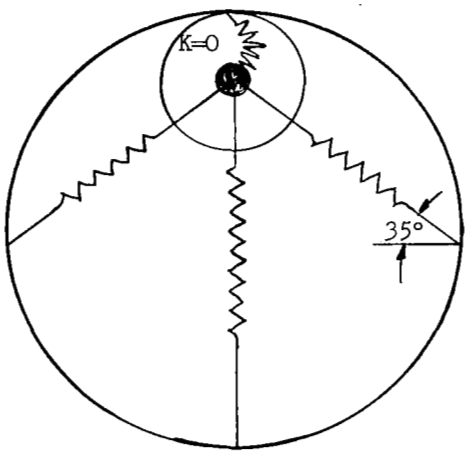

Case A

$K_{T_A} = K + 2K \sin 35°$

$K_{T_A} = 2.14K$

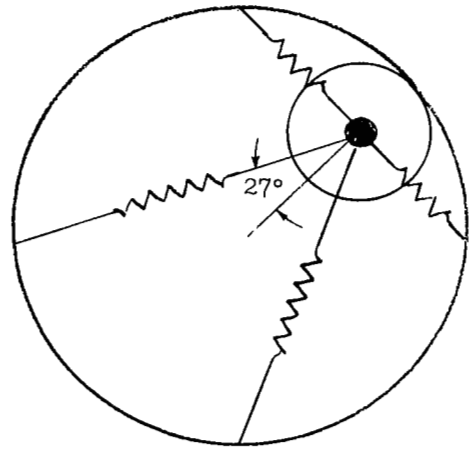

Case B

$K_{T_B} = 2K \cos 27°$

$K_{T_B} = 1.78K$

In case A the total spring constant, K_T, is .14/2.0 = 7% high. In case B the total spring constant K_T is .22/2.0 = 11% low. Thus the frequency ($\sim \sqrt{K_T}$) varies by about $\pm$ 5% around the desired value.

Bellows Design

Fluid volume = $V = \frac{\pi}{4} (D^2 - d^2)h$

$\Delta V = \alpha \Delta T \, V$

α = .00096/°C (Dow 200-210 fluids)

ΔT = 157°C = temperature range

$\Delta V = .00096 \, (157)(\frac{3.14}{4}) \, \{D^2 - (2.08)^2\}h$

$\Delta V = .1181 \, h \, \{D^2 - 4.32\}$

D = 6.00 in

h = 2.00 in

$\Delta V = .1181 \, (2.00) \, \{36.00 - 4.32\} = 7.52 \text{ in}^3$

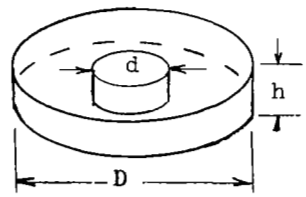

Assume $D_B = D - 1.00 = 5.0$ in

$$A_B = \frac{3.14}{4} D_B^2$$

$$\Delta V = A_B S \qquad (S = \text{stroke})$$

$$N = \frac{S}{\delta} = \frac{\text{Stroke}}{\text{Stroke per convolution}}$$

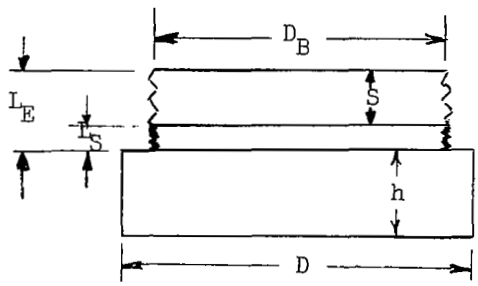

Let $\delta = .060$ in

Stacked length $= L_S = 3\ t\ N$

$$S = \frac{7.52 \times 4}{25 \times 3.14} = .384 \text{ in}$$

$N = .384/.060 = 6.4$; use $N = 7$

Let $t = .005$, then $L_S = 3\ (.005)\ (7) = .105$ in

$L_E = L_S + S = .384 + .105 = .489$ = extended length

The bellows are to be made of 347 stainless steel because of its good weldability and strength. Since the pressure buildup during sterilization will govern the housing size, the bellows spring rate will be limited to 200 lb/in.

Stress Analysis

During the sterilization cycle the load in the bellows is

$$P = K_B S = 200 \text{ lb/in} \times .384 \text{ in} = 76.8 \text{ lb}$$

$$\text{Pressure} = p = \frac{P}{A_B} = \frac{76.8}{(\frac{3.14}{4})(25)} = 3.87 \text{ psi}$$

For a simply supported circular plate under lateral pressure

$$\sigma_{max} = \frac{3}{8} \times \frac{p' A_B \mu}{\pi t^2} \left(\frac{3}{\mu} + 1\right)$$

With a factor of safety - F.S. = 1.5

$p' = p \times F.S. = 1.5p$

$$\sigma_{max} = \frac{3d^2 p' \mu}{32t^2} \left(\frac{3}{\mu} + 1\right) = \sigma_{ult}$$

For 347 stainless steel, $\sigma_{ult} \simeq 95{,}000$ psi

$$t = \sqrt{\frac{3(6)^2(1.5)(3.87)(.3)}{32\ (95{,}000)}\ (11)} = .0262 \text{ in}$$

Since some fixity in the edges is present and thus some induced bending load is also present, t = .032 is assumed.

Viscous Damping

Assume laminar boundary layer theory

force = shear stress x area = $\mu \frac{\dot{\eta}}{\Delta} A$

μ = dynamic viscosity

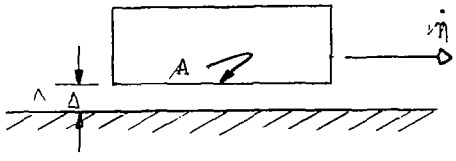

from the study results

$$\zeta = 2;\ \frac{c}{c_c} = 2;\ c_c = 2\omega m_2$$

where m_2 = mass; ω = undamped natural frequency

$$\text{force} = c\dot{\eta} = 4\omega\dot{\eta}m_2$$

thus $\mu = 4\omega m_2 \frac{\Delta}{A}$

for 4 lb and 1 cps damper

$$\mu = 4 \times 1 \times 6.28 \times \frac{4}{32.2} \frac{\Delta}{A} = 3.12 \frac{\Delta}{A} \frac{\text{lb. sec.}}{\text{ft}}$$

assume all surfaces of the two discs are effective and an effective gap, Δ, of .040 at each surface, thus

$$\mu = 3.12 \times \frac{.040 \times 12}{4 \times \frac{\pi}{4} (2.08)^2} = .114 \text{ lb sec/ft}^2$$

Dow Corning 200 series fluids have a weight density of .03515 lb/in^3 thus a kinematic viscosity, ν, of

$$\nu = \frac{\mu}{\rho} = \frac{.114 \times 32.2}{.03515 \times 1728} = .0604 \text{ ft}^2/\text{sec}$$

ν = 5450 centistokes is required

where

1 centistoke = 1 cm^2/sec

The vibrations experienced upon entry (boundary layer noise, etc.) will be such to alleviate damper stiction that might cause cg offset after oscillations have been eliminated.

Weight Analysis

1) Housing (γ = .282 lb/in^3 for 347 stainless steel)

$$W_H = .032 \left\{2\left(\frac{3.14}{4}\right) (6.00)^2 + 3.14\ (6.00)\ (2.12)\right\}\ (.282) = .862 \text{ lb}$$

2) Bellows

W_B = .30 lb (estimated)

3) Discs (γ = .700 lb/in^3 for tungsten)

$$W_D = 2\ (.84)\ \left(\frac{3.14}{4}\right)\ (2.08)^2\ (.700) = 4.00 \text{ lb}$$

4) Springs - Fittings - Port - Rubber

W_E = .10 lb (estimated)

5) Fluid (γ = .03515 lb/in^3 for Dow 200-210 fluids)

$$W_F = .03515 \left\{2.00\ \left(\frac{3.14}{4}\right)\ (5.90)^2 - 5.72\right\} = 1.71 \text{ lb}$$

Total

$$W_T = .86 + .30 + 4.00 + .10 + 1.71 = 6.97 \text{ lb}$$

3.3.2 10" Free Travel Length Damper

The 10 inch damper is similar to the other damper except that the extension springs are replaced by two spiral springs that deflect due to bending. Again, tungsten discs are used for the mass and a bellows accumulator is necessary.

Spiral Spring Design

Two spiral springs are required so that there is no net base moment acting on the body. Since the springs are in parallel, each spring must have half the desired rate or .204 lb/in each. Two wraps are assumed to give an omnidirectional spring constant. The spiral is clamped at the outside edge, is assumed to be round music wire and is analyzed as a series of semi-circular beams.

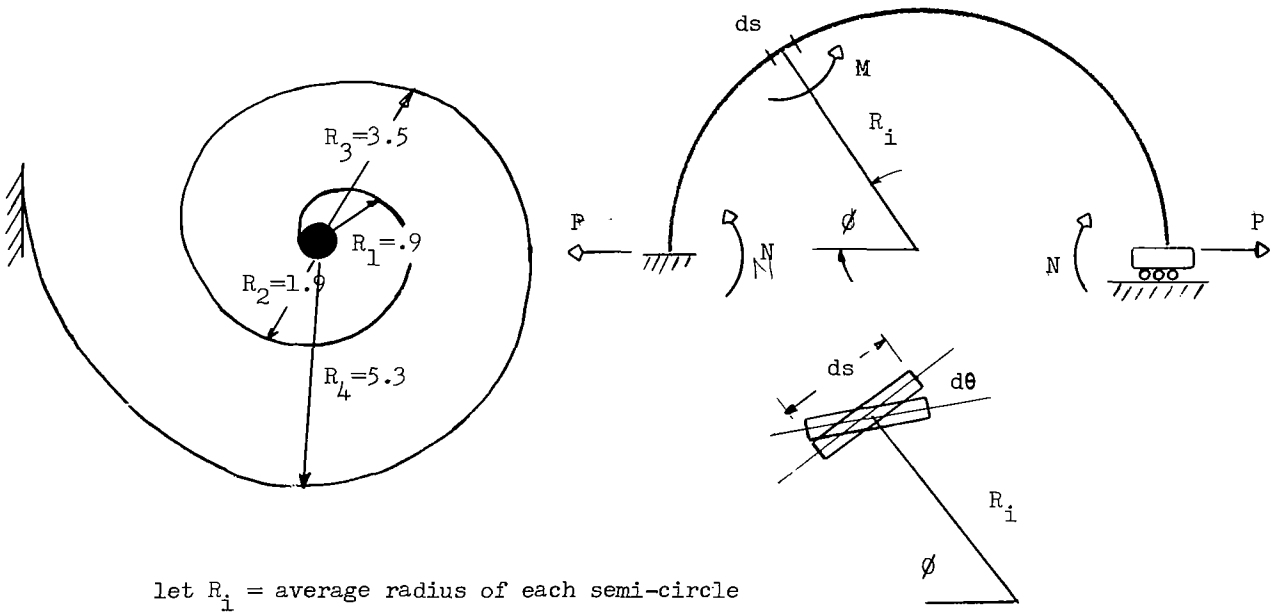

let R_i = average radius of each semi-circle

assume each semi-circle has fixed ends

then from the sketch

$$L = \pi\Sigma R_i = 38 \text{ in.} \qquad \frac{d\theta}{ds} = \frac{M}{EI} = \frac{PR_i \sin \phi - N}{EI} \; ; \; ds = R_i d\phi$$

where

$d\theta$ = incremental bending deflection

ds = incremental arc length

P = load in horizontal direction

N = base moment

M = moment in beam at location R,ϕ

EI = stiffness properties of beam

then the beam rotation, θ, at any location ϕ, is

$$\theta = \int_0^{\theta} d\theta = \frac{PR_i}{EI} \int_{\pi/2}^{\phi} (R_i \sin \phi - N)\, d\phi$$

$$\theta = + \frac{PR_i^2}{EI} \cos \phi + \frac{NR_i}{EI} \left(\phi - \frac{\pi}{2}\right)$$

$$\theta = 0 \text{ @ } \phi = 0 \text{ and } \phi = \pi$$

therefore $N = \frac{2}{\pi} PR_i$ is the base moment

and

$$\theta = + \frac{PR_i^2}{EI} \left[\cos \phi + \frac{2\phi}{\pi} - 1\right]$$

The total deflection in the horizontal direction, Δ, is

$$\Delta = \int_0^{\Delta} d\Delta = \int \theta ds \cos \phi = + \frac{PR_i^3}{EI} \int_0^{\pi} \left[\cos \phi + \frac{2\phi}{\pi} - 1\right] d\phi$$

$$\Delta = \frac{PR_i^3}{EI} \left[\frac{\pi}{2} - \frac{4}{\pi}\right] = \lambda \frac{PR_i^3}{EI} \quad \text{where } \lambda \simeq .3$$

Thus the spring rate for the complete spiral assuming 4 clamped semi-circles in series is

$$K = \frac{P}{\Sigma\Delta} = \frac{EI}{\lambda[R_1^3 + R_2^3 + R_3^3 + R_4^3]}$$

Similar analyses for pinned semicircles give the same expression with the value of $\lambda = \pi/2 = 1.57$. Also, analyses considering displacement in the vertical direction give values of λ within this range. For the following calculations, use $\lambda = .65$ (approximate geometric mean). From the above

$$I = \frac{\lambda K [R_1^3 + R_2^3 + R_3^3 + R_4^3]}{E}$$

for a round wire

$$I = \frac{\pi d^4}{64} = \frac{(.65)(.204)(189)}{30 \times 10^6} = .8 \times 10^{-6} \text{ in}^4$$

and

$$d = .0635 \text{ in}$$

is the wire diameter required.

The maximum stress is at the base and is given by the following

$$\sigma = \frac{M}{I}\frac{d}{2} = \frac{2}{\pi} \times \frac{PR}{I} \times \frac{d}{2}$$

$$= \frac{2}{\pi} \frac{(.204)\ 5 \times 6\ (.0317)}{.8 \times 10^{-6}} = 154{,}000 \text{ psi}$$

Bellows Design

$\Delta V = .1181\ (2.00)\ (144-4.32) = 33.0 \text{ in}^3$

$D_B = 11.00$ in

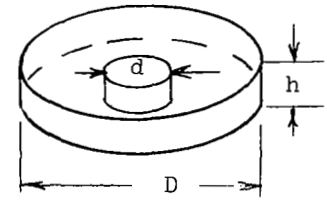

$$S = \frac{33.0}{\frac{3.14}{4}\ (121)} = .346 \text{ in}$$

$$N = \frac{.346}{.060} = 5.8; \text{ use } N = 6 \text{ convolutions}$$

$t = .005$ in

$L_S = S + L_S = .346 + .090 = .436$ in

Stress Analysis

If $K_B = 200$ lb/in

$P = 200\ (.346) = 69.3$ lb

$$p = \frac{69.3}{(\frac{3.14}{4})\ (121)} = .73 \text{ psi}$$

Factor of safety - F.S. = 1.5

Again for a simply supported flat plate

$$t = \sqrt{\frac{3(12)^2\ 1.5(.73)\ (.3)}{32\ (95000)}} = .0215 \text{ in}$$

use = .032 because of edge fixity uncertainty

Viscous Damping

$\zeta = \frac{1}{2}$ from the study, thus

$$\mu = \frac{3.12}{4} \frac{\Delta}{A} = .77 \frac{\Delta}{A} \text{ lb sec/ft}^2$$

assume all four surfaces effective and effective gap of .040 at each surface thus

$$\mu = .77 \frac{.040 \times 12}{4 \times 3.14 \ (1.04)^2} = .029 \text{ lb sec}^2/\text{ft}^2$$

Using a Dow 200 series fluid a kinematic viscosity of

$$\nu = \frac{.029}{.03515} \times \frac{32.2}{1728} = .01485 \text{ ft}^2/\text{sec}$$

$$= 1335 \text{ centistokes is required}$$

Weight Analysis

1) Housing

$$W_H = .032 \left\{2 \left(\frac{3.14}{4}\right) (12.00)^2 + 3.14 \ (12.00) \ (2.06)\right\} .282 = 2.73 \text{ lb}$$

2) Bellows

$$W_B = 1.0 \text{ lb (estimated)}$$

3) Discs

$$W_D = 4.00 \text{ lb}$$

4) Springs - Fittings - Ports - Rubber

$$W_E = .50 \text{ lb (estimated)}$$

5) Fluid

$$W_F = .03515 \left\{2.00 \left(\frac{3.14}{4}\right) (11.88)^2 - 5.72\right\} = 7.60 \text{ lb}$$

Total

$$W_T = 2.73 + 1.0 + 4.00 + .50 + 7.60 = 15.83 \text{ lb}$$

REFERENCES

1. "A Proposed Solution to the Entry Vehicle Design Penalties Caused by Lack of Knowledge of the Mars Atmosphere," George Levin, NASA Goddard Space Flight Center, AIAA Paper 65-493 AIAA 2nd Annual Meeting, San Francisco, California, July 26-29, 1965.

2. Selected entry probe trajectory listings generated by a six-degree-of-freedom digital computer program. This data provided as needed during 1965 by the technical monitor, Mr. George Levin, NASA Goddard Space Flight Center.

3. "NASA Engineering Models of the Mars Atmosphere for Entry Vehicle Design," NASA TN D-2525 edited by G. M. Levin, D. E. Evans and V. Stevens, November 1964.

APPENDIX I

This appendix contains a portion of the analog schematics used in the study. The intent is to show how the equations of motion, the impact conditions, and the logic were wired on the patchboard. The schematics shown are for the initial set of simulations, that is, the 21,800 ft/sec and 19,200 ft/sec entries with both the 3" and 10" free travel length. The units used were foot, lb, seconds and the problem was run in real time. The grazing entry required rescaling the dynamic pressure loop (A40, $\overline{A12}$, A25). The deeper entries required amplitude and time scaling both coordinate loops and replacement of the exponential atmosphere simulation (A40 etc) with a function generator. This latter change was necessary since the βV_v product (P110) was not constant.

The analog schematics and simulation are briefly summarized in the following paragraphs. As mentioned earlier multiple clocks were used. The clocks govern the integrator operation. The "η loop" clock controlled only the integrators in the η integration cycle (A56, A57, $\overline{A58}$, $\overline{A59}$). All other integrators were controlled by the α clock. The super bar on the amplifier, e.g., $\overline{A58}$, indicates that it is a complimentary integrator and operates as described in Section 2.3. The clocks are stopped and started by grounding certain of their inputs. This is indicated on Figures I-1 and I-3.

The top row of operations indicated as Figure I-1 is the α loop and integrates the $\ddot{\alpha}$ equation. The second row is a similar η loop. The connections through the potentiometers and multipliers (P05, M00, M13) are the impact conditions. In the α loop the initial condition on angular rate is on P06. The free travel length is set on P129. The spring rate, damping coefficient and coefficient of restitution are set on P201, P203, P202 respectively.

The schematic on Figure I-2 shows the aerodynamic terms. The aerodynamic coefficients are generated using function generators (FG) and are sign changed through a relay since they are symmetric about $\alpha = 0$. The dynamic pressure, q, is exponentially generated (A40, $\overline{A12}$, A25) with P010 set at q_o and P110 set at the βV_v value.

After collision at the boundary ($\eta = \pm\eta_M$), relay K02, Figure I-1, is thrown and stops both clocks. The logic, Figure I-3 ensures that after about a second the α clock is started automatically (A69, $\overline{A43}$, K03). During that time the new damper rate, $\dot{\eta}_a$, is checked for magnitude (A21...A70). If $\dot{\eta} \neq 0$, relay K01 is thrown to the "bounce" position and then both the η and α clocks are automatically started. If however $\dot{\eta} = 0$ ($\epsilon = 0$) then the η clock is not started with the α clock since relay K01 is in the "stick" position. During the ensuing solution of the α loop the value of $\ddot{\eta}$ is monitored, and when $\ddot{\eta}$ amd η are of opposite sign (A65, A46...K05) relay K05 is thrown to the "release" position and the η clock is started. The solution of both loops is now continued to the next impact.

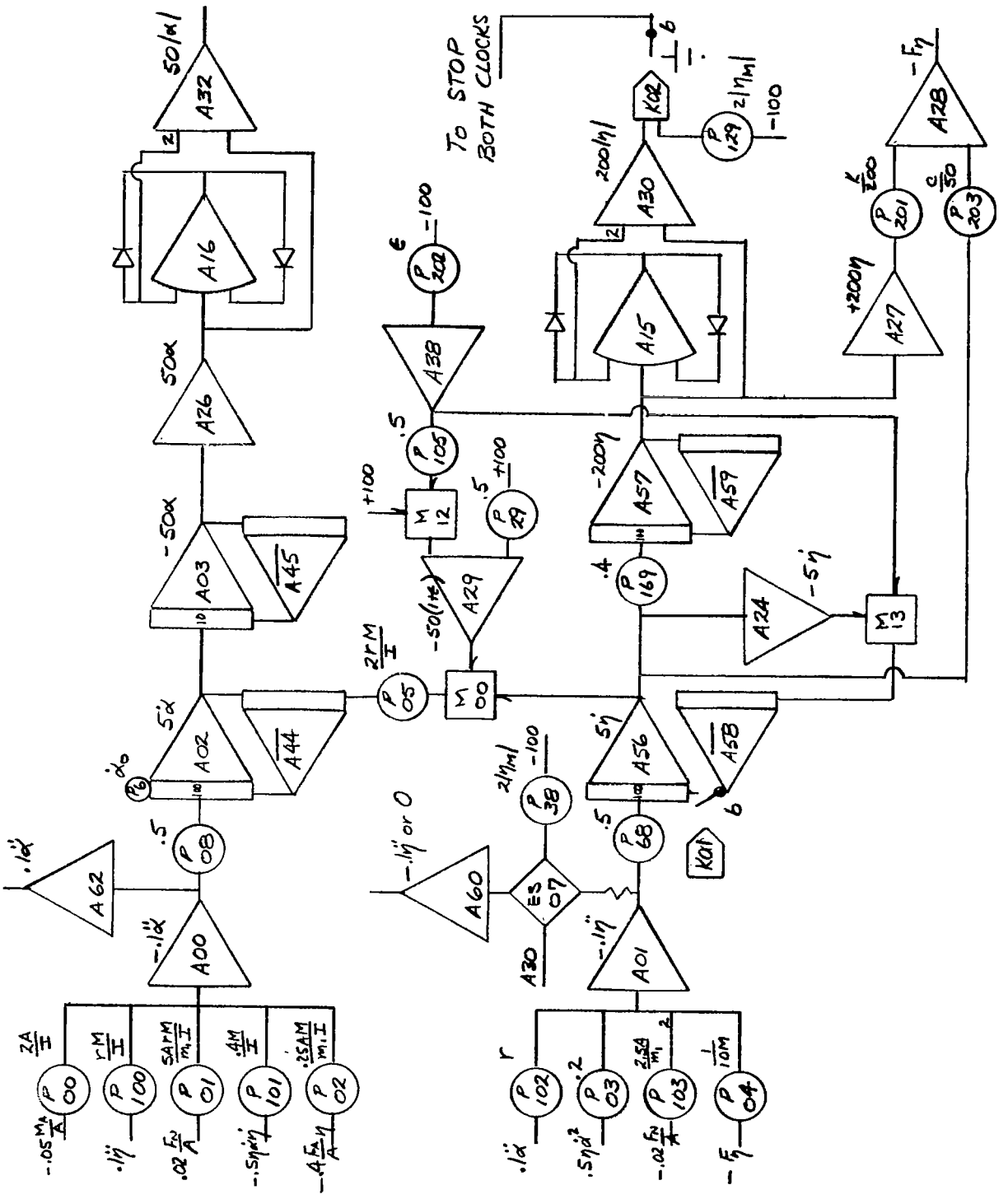

FIGURE I-1 α and η Loops

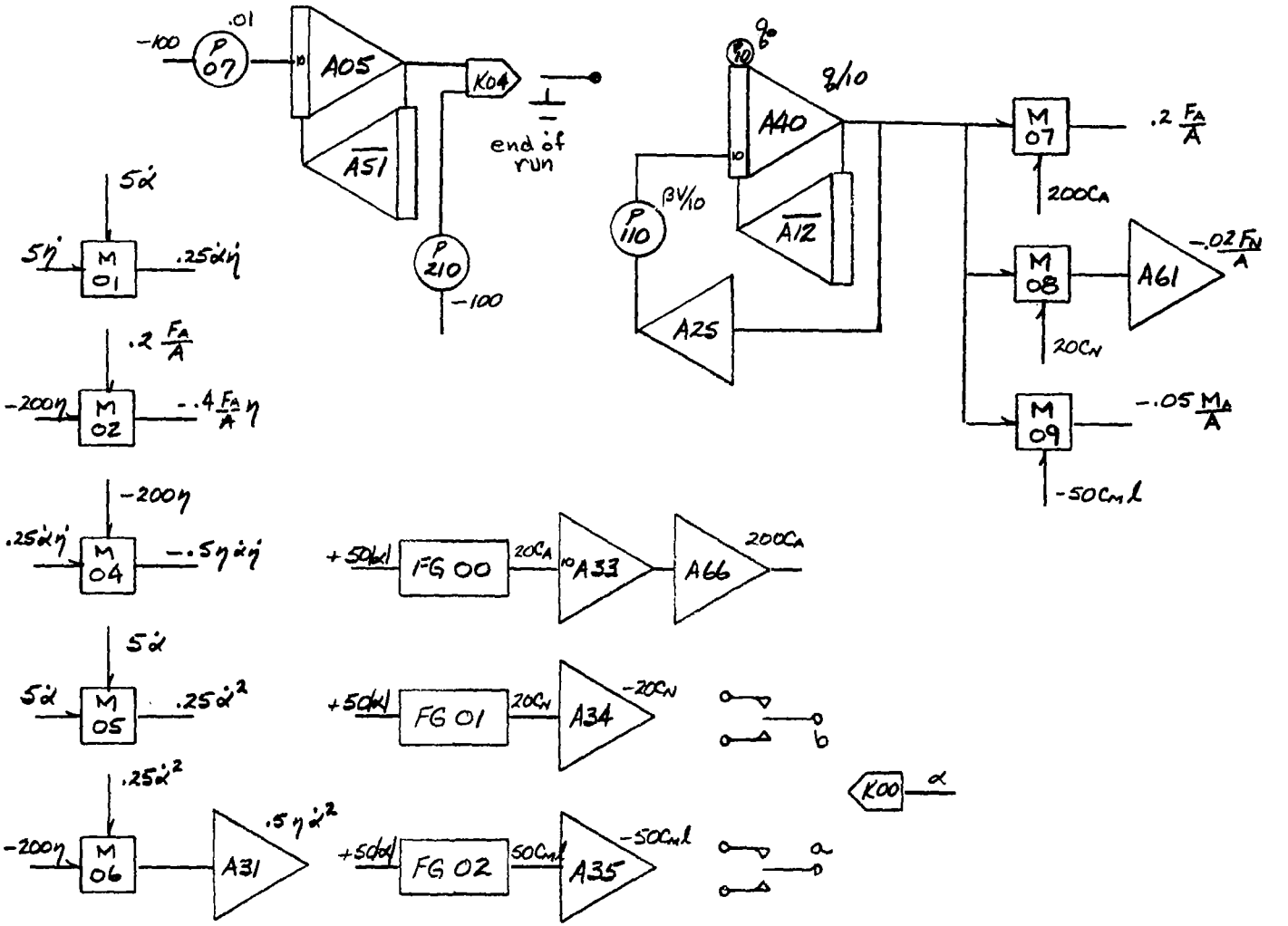

FIGURE I-2 Aerodynamics

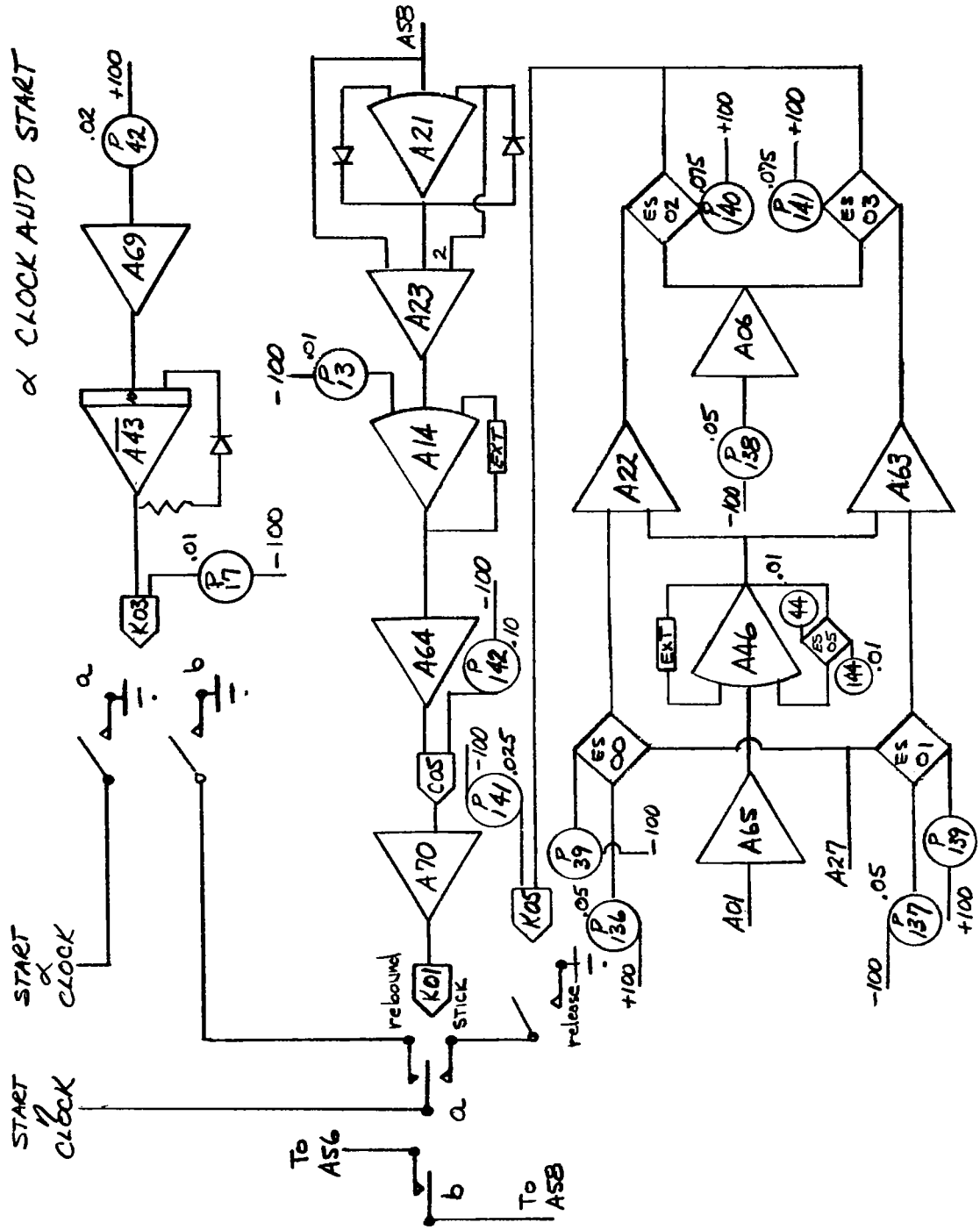

FIGURE I-3 Logic

APPENDIX II

Presented as Appendix II are the tabulated results of the analog computer runs. The data is catagorized by trajectory entry velocity and damper mass free travel length. The data is presented as points on angle-of-attack envelopes at several altitudes for various damper parameters. This is done for each of the four initial conditions on $\dot{\alpha}_o$ for each trajectory.

Tables II-1, and II-2 give data on the original 21,800 ft/sec entry velocity trajectory. Tables II-3 and II-4 give similar data for the 19,200 ft/sec entry velocity trajectory. The data in Tables II-5 and II-6 is for the grazing entry (approximately 16° down) at 15,000 ft/sec. Since this was not the primary trajectory the number of runs was reduced by excluding some damper frequency and initial rate variations. Since the frequency of oscillation is lower for this trajectory (due to lower q at any altitude) an additional damper frequency was considered, 1/2 cps. This actually was more effective for this trajectory than the selected damper. However it was not considered in the other simulations.

In some cases the angle-of-attack envelope with the damper system appears higher than that of the basic trajectories. This may be so for three reasons as commented on below.

1) The analog simulations were initiated with angular rates equal to those taken from a basic trajectory with no damper system. Since the damper mass is approximately 10% of the total weight, this additional weight gives the simulated probe additional energy. Thus for the first one or two cycles, if the damper is not effective, the envelope is higher.

2) The scaling of the analog computer is subject to the following conditions. The dynamic pressure q must be scaled to the high value at the end of the trajectory. On the other hand, the vehicle angular rate and the damper mass velocity must be scaled to the case where the damper is not effective and the rates are high. The analog equipment is more accurate of course, using higher voltages and thus is best towards the end of a basic trajectory. Small inherent variations in voltages (e.g., loading initial condition voltages) are more pronounced early in flight.

3) Certain phasings of impacts might actually increase the angle-of-attack over portions of the flight. This would occur when the mass would impact at an extreme of angular displacement, (and thus close to the null angular rate) and thus the rate transfer would cause the angular position to continue to increase rather than return.

A combination of the above in an unpredictable manner for the large number of runs restricts data accuracy to, at best, 1° towards the end of the simulations.

There are three explanatory comments to assist in using the tables. First the symbol (-) indicates that the data was not obtained, and secondly, the sumbol (+) indicates that one or no impacts occurred so that following runs with only an ε variation would give the same results. Third, the data used in preparing Figures 8-17 are shown outlined in the tables.

TABLE II-1. V=21,800 ft/sec., 3" Free Travel Length, θ = 90 deg.

Undamped Trajectory			α_i = 155 deg, $\dot{\alpha}_o$ = 2.4 rad/sec				α_i = 138 deg, $\dot{\alpha}_o$ = 1.8 rad/sec			
			Altitude (KFT)				Altitude (KFT)			
			125	100	85	50	125	100	85	50
			Angle-of-Attack (Deg.)				Angle-of-Attack (Deg.)			
			38	29	26	20	31	24	20	16
Damper Parameter										
f=1	ζ=0	ϵ=0	39	32	28	-	28	21	18	-
		.5	40	30	20	-	30	21	-	-
		1.0	40	33	28	-	30	24	21	-
	.5	0	39	29	26	25	30	22	16	15
		.5	40	28	18	18	30	20	13	13
		1.0	38	28	26	14	29	20	16	8
	1.0	0	38	29	25	24	29	20	17	14
		.5	39	29	21	21	30	22	14	13
		1.0	34	23	19	7	26	18	14	5
	2.0	0	39	29	27	24	28	20	17	12
		.5	39	30	24	23	29	21	16	8
		1.0	30	16	13	4	26	13	8	3
	4.0	0	38	28	24	19	28	19	15	7
		.5	39	29	24	21	27	17	10	4
		1.0	36	17	10	3	26	12	7	2
3	0	0	40	30	27	-	30	22	19	-
		.5	40	30	25	-	31	22	16	-
		1.0	40	32	28	-	31	24	23	-
	.5	0	39	30	26	-	31	22	20	-
		.5	41	32	26	-	32	24	16	-
		1.0	38	26	22	-	31	22	-	-
	1.0	0	39	28	26	-	30	22	18	-
		.5	40	32	26	-	30	22	18	-
		1.0	40	24	17	-	28	18	8	-
	2.0	0	38	28	24	-	28	19	15	-
		.5	40	30	24	-	-	-	-	-
		1.0	38	27	16	-	28	16	9	-
5	0	0	40	31	29	-	30	22	20	-
		.5	40	31	26	-	30	24	21	-
		1.0	39	31	29	-	30	24	21	-
	.5	0	38	31	28	-	29	22	20	-
		.5	40	-	-	-	30	24	20	-
		1.0	40	29	22	-	29	22	16	-

TABLE II-1 (Cont'd)

Undamped Trajectory			$\alpha_i = 109$ deg, $\dot{\alpha}_o = 1.2$ rad/sec				$\alpha_i = 57$ deg, $\dot{\alpha}_o = 0.6$ rad/sec			
			Altitude (KFT)				Altitude (KFT)			
			125	100	85	50	125	100	85	50
			Angle-of-Attack (Deg.)				Angle-of-Attack (Deg.)			
			20	16	13	10	11	8	6	5
Damper Parameter										
f=1	ζ=0	ε=0	20	13	8	-	8	2	1	-
		.5	19	10	6	-	8	2	1	-
		1.0	20	15	13	-	9	6	5	-
	.5	0	18	11	7	-	9	3	2	-
		.5	18	9	7	-	9	3	1	-
		1.0	18	11	9	-	8	4	2	-
	1.0	0	18	12	9	-	9	4	2	-
		.5	18	10	5	-	8	3	2	-
		1.0	18	10	6	-	9	4	2	-
	2.0	0	18	11	7	-	9	4	2	-
		.5	18	10	5	-	-	-	-	-
		1.0	17	9	4	-	9	4	2	-
	4.0	0	-	-	-	-	-	-	-	-
		.5	-	-	-	-	-	-	-	-
		1.0	-	-	-	-	-	-	-	-
3	0	0	20	15	11	-	9	6	4	-
		.5	21	14	9	-	9	7	5	-
		1.0	20	17	14	-	10	8	6	-
	.5	0	19	12	10	-	10	5	3	-
		.5	20	16	-	-	10	5	3	-
		1.0	20	13	9	-	10	5	3	-
	1.0	0	20	13	9	-	-	-	-	-
		.5	19	12	8	-	-	-	-	-
		1.0	18	11	6	-	-	-	-	-
	2.0	0	-	-	-	-	-	-	-	-
		.5	-	-	-	-	-	-	-	-
		1.0	-	-	-	-	-	-	-	-
5	0	0	20	16	12	-	12	7	6	-
		.5	21	17	12	-	10	8	6	-
		1.0	21	17	14	-	11	8	7	-
	.5	0	20	16	11	-	10	7	6	-
		.5	-	-	-	-	-	-	-	-
		1.0	19	14	12	-	-	-	-	-

TABLE II-2. V=21,800 ft/sec., 10" Free Travel Length, θ = 90 deg.

Undamped Trajectory			α_j = 155 deg, $\dot{\alpha}_o$ = 2.4 rad/sec				α_j = 138 deg, $\dot{\alpha}_o$ = 1.8 rad/sec			
			Altitude (KFT)				Altitude (KFT)			
			125	100	85	50	125	100	85	50
			Angle-of-Attack (Deg.)				Angle-of-Attack (Deg.)			
			38	29	26	20	31	24	20	16
Damper Parameter										
f=1	ζ=0	ϵ=0	39	21	9	-	24	11	3	-
		.5	36	19	9	-	23	10	4	-
		1.0	40	31	28	-	30	21	18	-
	.5	0	34	18	8	-	24	10	4	-
		.5	32	13	4	-	23	8	2	-
		1.0	32	20	12	-	23	11	5	-
	1.0	0	33	16	6	-	23	10	4	-
		.5	32	14	3	-	23	10	4	-
		1.0	30	15	5	-	23	9	3	-
	2.0	0	35	18	8	-	+25	12	6	-
		.5	32	16	6	-	+24	11	6	-
		1.0	30	16	6	-	+24	11	6	-
3	0	0	40	25	15	-	30	19	11	-
		.5	40	26	16	-	30	21	14	-
		1.0	41	34	27	-	31	23	20	-
	.5	0	40	24	16	-	31	18	8	-
		.5	39	23	11	-	30	17	9	-
		1.0	40	24	14	-	30	18	10	-
	1.0	.0	39	21	15	-	+29	16	9	-
		.5	39	22	11	-	+29	16	9	-
		1.0	39	21	12	-	+29	16	9	-
5	0	0	41	31	24	-	+32	23	20	-
		.5	41	32	25	-	+32	23	21	-
		1.0	41	32	29	-	+32	23	22	-
	.5	0	41	29	23	-	+31	21	16	-
		.5	41	30	21	-	+31	21	16	-
		1.0	41	30	21	-	+31	21	16	-

TABLE II-2 (cont'd)

Undamped Trajectory			α_i = 109 deg, $\dot{\alpha}_o$ = 1.2 rad/sec				α_i = 57 deg, $\dot{\alpha}_o$ = 0.6 rad/sec			
			Altitude (KFT)				Altitude (KFT)			
			125	100	85	50	125	100	85	50
			Angle-of-Attack (Deg.)				Angle-of-Attack (Deg.)			
			20	16	13	10	11	8	6	5
Damper Parameter										
f=1	ζ=0	ε=0	16	4	2	-	6	2	1	-
		.5	17	7	3	-	8	2	1	-
		1.0	18	14	11	-	10	5	5	-
	.5	0	16	4	2	-	+ 7	2	1	-
		.5	15	4	2	-	-	-	-	-
		1.0	15	6	2	-	-	-	-	-
	1.0	0	16	6	2	-	+ 9	3	2	-
		.5	15	5	2	-	-	-	-	-
		1.0	15	5	2	-	-	-	-	-
	2.0	0	+18	8	4	-	+10	4	2	-
		.5	+18	8	4	-	-	-	-	-
		1.0	+18	8	4	-	-	-	-	-
3	0	0	20	14	-	-	+12	6	5	-
		.5	21	14	10	-	-	-	-	-
		1.0	21	14	11	-	-	-	-	-
	.5	0	+21	12	6	-	+11	6	3	-
		.5	+21	12	6	-	-	-	-	-
		1.0	+21	12	6	-	-	-	-	-
	1.0	0	+20	12	7	-	+11	6	3	-
		.5	+20	12	7	-	-	-	-	-
		1.0	+20	12	7	-	-	-	-	-
5	0	0	+20	16	13	-	+11	7	6	-
		.5	+20	16	13	-	-	-	-	-
		1.0	+20	16	13	-	-	-	-	-
	.5	0	+21	15	10	-	+11	7	6	-
		.5	+21	15	10	-	-	-	-	-
		1.0	+21	15	10	-	-	-	-	-

TABLE II-3. V=19,200 ft/sec., 3" Free Travel Length, θ = 90 deg.

Undamped Trajectory			α_i = 155 deg, $\dot{\alpha}_o$ = 2.1 rad/sec				α_i = 139 deg, $\dot{\alpha}_o$ = 1.6 rad/sec			
			Altitude (KFT)				Altitude (KFT)			
			125	100	85	50	125	100	85	50
			Angle-of-Attack (Deg.)				Angle-of-Attack (Deg.)			
			43	32	29	22	34	26	22	18
Damper Parameter										
f=1	ζ=0	ε=0	44	36	29	-	29	23	18	-
		.5	46	38	28	-	30	23	15	-
		1.0	44	36	32	-	35	28	24	-
	.5	0	44	35	29	28	34	26	21	19
		.5	46	35	25	25	35	27	19	17
		1.0	42	34	27	15	32	24	20	11
	1.0	0	45	35	29	28	34	25	20	17
		.5	46	38	29	28	34	27	20	17
		1.0	39	30	23	9	30	22	16	6
	2.0	0	44	35	28	26	34	26	20	15
		.5	46	36	28	27	34	26	20	10
		1.0	44	27	17	5	33	21	13	3
	4.0	0	43	35	28	22	34	24	20	12
		.5	43	35	28	25	33	24	17	7
		1.0	43	31	19	5	33	21	12	3
3	0	0	47	38	32	-	36	28	23	-
		.5	48	40	31	-	36	29	23	-
		1.0	46	39	33	-	35	28	25	-
	.5	0	47	36	30	-	36	27	22	-
		.5	48	38	32	-	36	28	24	-
		1.0	46	32	24	-	35	25	20	-
	1.0	0	46	36	30	-	35	26	22	-
		.5	47	37	32	-	35	28	22	-
		1.0	47	34	23	-	35	26	17	-
	2.0	0	45	34	28	-	34	26	20	-
		.5	45	34	26	-	34	26	19	-
		1.0	45	32	23	-	33	25	17	-
5	0	0	45	38	32	-	35	28	25	-
		.5	46	38	34	-	35	29	25	-
		1.0	46	38	33	-	35	28	25	-
	.5	0	46	36	31	-	34	27	23	-
		.5	46	37	33	-	35	28	25	-
		1.0	46	37	28	-	34	28	23	-

TABLE II-3 (cont'd)

Undamped Trajectory			α_i = 108 deg, $\dot{\alpha}_o$ = 1.05 rad/sec				α_i = 56 deg, $\dot{\alpha}_o$ = 0.5 rad/sec			
			Altitude (KFT)				Altitude (KFT)			
			125	100	85	50	125	100	85	50
			Angle-of-Attack (Deg.)				Angle-of-Attack (Deg.)			
			21	16	14	10	11	8	7	5
Damper Parameter										
f=1	ζ=0	ε=0	21	15	11	-	11	7	3	-
		.5	21	16	9	-	11	7	4	-
		1.0	23	20	17	-	12	10	10	-
	.5	0	22	17	12	-	11	7	3	-
		.5	22	15	9	-	11	6	3	-
		1.0	20	17	12	-	11	8	4	-
	1.0	0	22	17	12	-	11	7	3	-
		.5	22	16	10	-	11	6	2	-
		1.0	20	15	10	-	11	6	3	-
	2.0	0	22	16	11	-	+11	7	3	-
		.5	22	15	9	-	+11	7	3	-
		1.0	22	14	8	-	+11	7	3	-
	4.0	0	23	16	11	-	-	-	-	-
		.5	23	16	10	-	-	-	-	-
		1.0	22	15	8	-	-	-	-	-
3	0	0	24	19	14	-	12	10	7	-
		.5	24	19	12	-	12	10	7	-
		1.0	24	19	17	-	12	10	8	-
	.5	0	24	19	13	-	12	9	6	-
		.5	24	19	14	-	12	9	6	-
		1.0	24	18	13	-	12	9	5	-
	1.0	0	23	18	13	-	+12	9	5	-
		.5	23	18	13	-	+12	9	5	-
		1.0	23	18	11	-	+12	9	5	-
	2.0	0	23	18	12	-	-	-	-	-
		.5	23	18	13	-	-	-	-	-
		1.0	22	17	12	-	-	-	-	-
5	0	0	24	18	16	-	+12	9	8	-
		.5	24	18	16	-	+12	9	8	-
		1.0	24	19	16	-	+12	9	8	-
	.5	0	24	19	15	-	+12	9	7	-
		.5	24	19	16	-	+12	9	7	-
		1.0	24	19	15	-	+12	9	7	-

TABLE II-4. V=19,200 ft/sec., 10" Free Travel Length, θ = 90 deg.

Undamped Trajectory			α_i = 155 deg, $\dot{\alpha}_o$ = 2.1 rad/sec				α_i = 139 deg, $\dot{\alpha}_o$ = 1.6 rad/sec.			
			Altitude (KFT)				Altitude (KFT)			
			125	100	85	50	125	100	85	50
Damper Parameter			Angle-of-Attack (Deg.)				Angle-of-Attack (Deg.)			
f=1	ζ=0	ε=0	43	33	29	22	34	26	22	18
		.5	40	24	12	-	25	10	2	-
		1.0	36	16	10	-	24	11	4	-
	.5	0	41	32	29	-	30	24	20	-
		.5	34	15	5	-	24	9	4	-
		1.0	32	14	3	-	23	10	2	-
	1.0	0	34	20	12	-	24	12	6	-
		.5	34	15	7	-	26	13	6	-
		1.0	34	14	4	-	24	8	3	-
	2.0	0	30	12	5	-	24	9	3	-
		.5	38	20	10	-	28	17	8	-
		1.0	33	16	9	-	+26	12	7	-
3	0	0	32	16	9	-	-	-	-	-
		.5	42	28	18	-	32	21	15	-
		1.0	44	32	22	-	-	-	-	-
	.5	0	45	34	30	-	32	25	23	-
		.5	42	26	20	-	32	20	12	-
		1.0	42	26	19	-	-	-	-	-
	1.0	0	44	26	18	-	33	20	12	-
		.5	+42	25	14	-	+32	20	12	-
		1.0	-	-	-	-	-	-	-	-
	2.0	0	-	-	-	-	-	-	-	-
5	0	0	+43	28	19	-	+31	20	16	-
		.5	43	32	27	-	+32	24	21	-
		1.0	-	-	-	-	-	-	-	-
	.5	0	44	32	30	-	-	-	-	-
		.5	+44	31	22	-	+33	24	18	-
		1.0	-	-	-	-	-	-	-	-
	1.0	0	+44	31	23	-	-	-	-	-
		.5	+44	31	23	-	-	-	-	-
		1.0	-	-	-	-	-	-	-	-
	2.0	0	-	-	-	-	-	-	-	-
			-	-	-	-	-	-	-	-
			-	-	-	-	-	-	-	-
			+45	32	24	-	-	-	-	-

TABLE II-4 (cont'd)

Undamped Trajectory			α_i = 108 deg, $\dot{\alpha}_o$ = 1.05 rad/sec				α_i = 56 deg, $\dot{\alpha}_o$ = 0.5 rad/sec			
			Altitude (KFT)				Altitude (KFT)			
			125	100	85	50	125	100	85	50
			Angle-of-Attack (Deg.)				Angle-of-Attack (Deg.)			
			21	16	14	10	11	8	7	5
Damper Parameter										
f=1	ζ=0	e=0	16	6	1	-	8	1	1	-
		.5	17	9	2	-	10	4	1	-
		1.0	21	16	14	-	10	7	5	-
	.5	0	17	5	2	-	+ 8	2	1	-
		.5	16	6	2	-	-	-	-	-
		1.0	16	8	3	-	-	-	-	-
	1.0	0	18	6	2	-	+ 9	4	2	-
		.5	-	-	-	-	-	-	-	-
		1.0	18	6	2	-	-	-	-	-
	2.0	0	+18	8	2	-	+10	5	2	-
		.5	-	-	-	-	-	-	-	-
		1.0	-	-	-	-	-	-	-	-
3	0	0	22	16	11	-	+11	8	6	-
		.5	-	-	-	-	-	-	-	-
		1.0	23	16	12	-	-	-	-	-
	.5	0	+22	14	9	-	+12	8	5	-
		.5	-	-	-	-	-	-	-	-
		1.0	-	-	-	-	-	-	-	-
	1.0	0	+22	13	9	-	+12	8	6	-
		.5	-	-	-	-	-	-	-	-
		1.0	-	-	-	-	-	-	-	-
	2.0	0	-	-	-	-	-	-	-	-
5	0	0	+20	16	14	-	+11	8	7	-
		.5	-	-	-	-	-	-	-	-
		1.0	-	-	-	-	-	-	-	-
	.5	0	+22	16	14	-	+12	8	7	-
		.5	-	-	-	-	-	-	-	-
		1.0	-	-	-	-	-	-	-	-
	1.0	0	-	-	-	-	-	-	-	-
		.5	-	-	-	-	-	-	-	-
		1.0	-	-	-	-	-	-	-	-
	2.0	0	-	-	-	-	-	-	-	-

TABLE II-5. V=15,000 ft/sec., 3" Free Travel Length, θ = 16 deg.

Undamped Trajectory			α_i = 180 deg, $\dot{\alpha}_o$ = 0.8 rad/sec			α_i = 72 deg, $\dot{\alpha}_o$ = 0.4 rad/sec		
			Altitude (KFT)			Altitude (KFT)		
			200	150	115	200	150	115
			Angle-of-Attack (Deg.)			Angle-of-Attack (Deg.)		
			75	46	32	38	24	16
Damper Parameter								
f=½	ζ=0	ε=0	75	40	23	38	-	-
		.5		49	22		-	-
		1.0		45	33		23	15
	.25	0		43	30		20	9
		.5		46	25		18	5
		1.0		40	26		22	12
	.5	0		42	26		20	9
		.5		44	28		18	5
		1.0		37	18		19	9
	1.0	0		42	26		12	4
		.5		44	25		12	2
		1.0		26	10		13	4
	2.0	0		41	25		11	2
		.5		43	28		11	2
		1.0		35	8		11	2
1	0	0		46	30		22	9
		.5		48	25		23	7
		1.0		48	34		23	16
	.25	0		46	30		22	9
		5		48	30		22	9
		1.0		44	27		22	9
	.5	0		46	30		21	8
		.5		47	29		24	9
		1.0		40	18		22	8
	1.0	0		42	25		21	6
		.5		47	31		22	6
		1.0		42	12		21	5
	2.0	0		44	26		20	7
		.5		45	28		20	7
		1.0	75	42	13	38	20	7

TABLE II-6. V=15,000 ft/sec., 10" Free Travel Length, θ = 16 deg.

Undamped Trajectory			α_i = 180 deg, $\dot{\alpha}_o$ = 0.8 rad/sec			α_i = 72 deg, $\dot{\alpha}_o$ = 0.4 rad/sec		
			Altitude (KFT)			Altitude (KFT)		
			200	150	115	200	150	115
			Angle-of-Attack (Deg.)			Angle-of-Attack (Deg.)		
			75	46	32	38	24	16
Damper Parameter								
f=½	ζ=0	ε=0	75	31	1	38	14	-
		.5		27	1		15	-
		1.0		46	32		23	14
	.25	0		32	2		12	0
		.5		27	1		12	1
		1.0		25	2		14	1
	.5	0		29	1		11	0
		.5		22	1		11	1
		1.0		20	1		12	1
	1.0	0		25	2		+13	1
		.5		22	2		-	-
		1.0		16	2		-	-
	2.0	0		+26	5		-	-
		.5		+26	5		-	-
		1.0		+26	5		-	-
1	0	0		38	9		20	9
		.5		38	9		22	11
		1.0		41	30		25	15
	.25	0		34	6		+20	5
		.5		36	6		+20	5
		1.0		36	10		+20	5
	.50	0		33	5		+18	4
		.5		32	4		-	-
		1.0		33	4		-	-
	1.0	0		+32	5		+20	5
		.5		+32	5		-	-
		1.0		+32	5		-	-
	2.0	0		+35	11		-	-
		.5		+35	11		-	-
		1.0	75	+35	11	38	-	-

NASA-Langley, 1966 CR-525